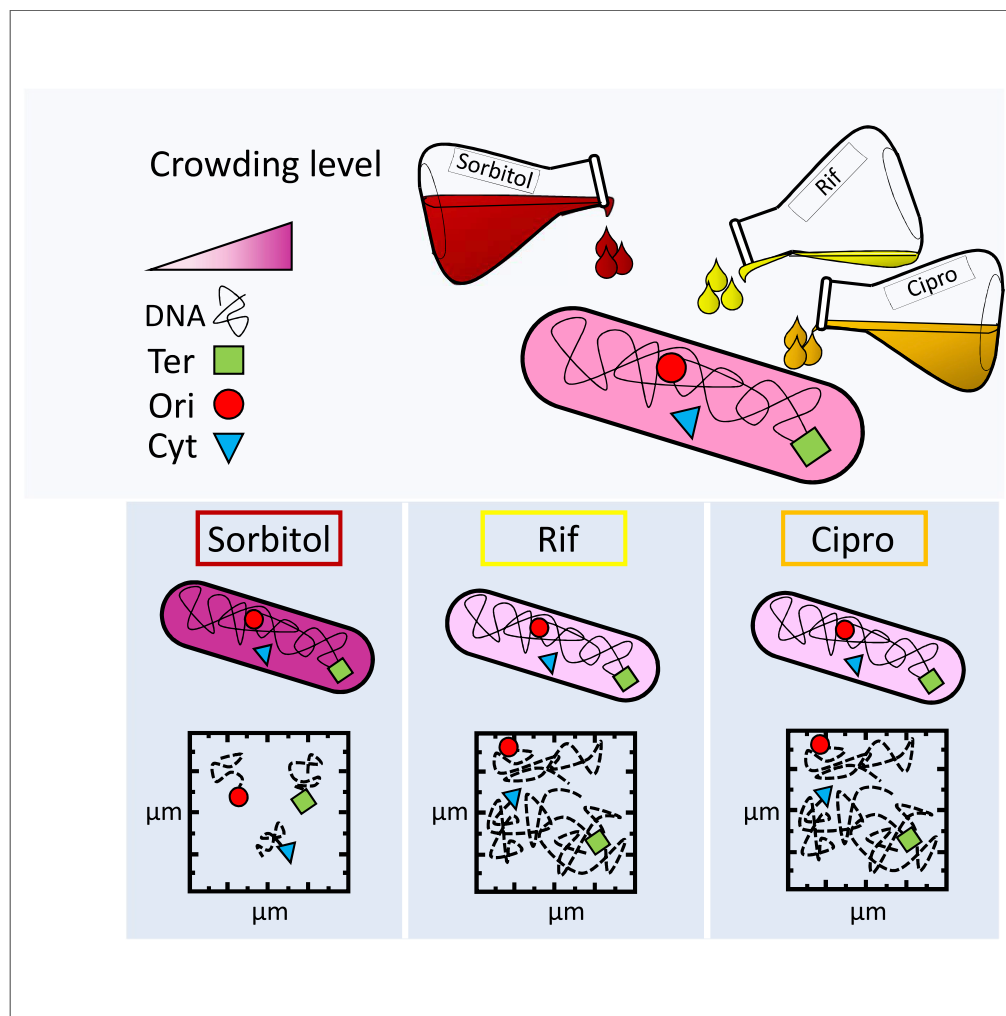## Article

Cytosolic Crowding Drives the Dynamics of Both Genome and Cytosol in *Escherichia coli* Challenged with Sub-lethal Antibiotic Treatments

Michal Wlodarski,
Leonardo Mancini,
Bianca Raciti,
Bianca Sclavi,
Marco Cosentino
Lagomarsino,
Pietro Cicuta

marco.
cosentino-lagomarsino@ifom.
eu (M.C.L.)
pc245@cam.ac.uk (P.C.)

HIGHLIGHTS

Motility of loci positioned on different parts of the chromosome is correlated to sub-lethal antibiotic treatments

Motility changes of chromosomal loci correlate with those of cytosolic aggregates

Treatment-induced changes to crowding levels in cytosol are consistent with the changes in motility

Article

Cytosolic Crowding Drives the Dynamics of Both Genome and Cytosol in *Escherichia coli* Challenged with Sub-lethal Antibiotic Treatments

Michal Wlodarski,[1,5,6] Leonardo Mancini,[1,6] Bianca Raciti,[1] Bianca Sclavi,[2] Marco Cosentino Lagomarsino,[3,*] and Pietro Cicuta[4,*]

SUMMARY

In contrast to their molecular mode of action, the system-level effect of antibiotics on cells is only beginning to be quantified. Molecular crowding is expected to be a relevant global regulator, which we explore here through the dynamic response phenotypes in *Escherichia coli*, at single-cell resolution, under sub-lethal regimes of different classes of clinically relevant antibiotics, acting at very different levels in the cell. We measure chromosomal mobility through tracking of fast (<15 s timescale) fluctuations of fluorescently tagged chromosomal loci, and we probe the fluidity of the cytoplasm by tracking cytosolic aggregates. Measuring cellular density, we show how the overall levels of macromolecular crowding affect both quantities, regardless of antibiotic-specific effects. The dominant trend is a strong correlation between the effects in different parts of the chromosome and between the chromosome and cytosol, supporting the concept of an overall global role of molecular crowding in cellular physiology.

INTRODUCTION

Antibiotic perturbations cause an interplay of physiological responses and specific responses to treatment; in general, this is still an open question, with potential impact in the biomedical field. Although the molecular mechanisms of action of most antibiotics are well known, their effects on the physiology of the cell at a "systems" level remain largely unexplored. For example, we currently cannot predict the precise effects of treatments on gene expression patterns. These changes that affect the cell as a system may be due to physical aspects of the cell state, such as the levels of molecular crowding and the compaction state of the genome (Pelletier et al., 2012). Crowding, for example, may affect both genome compaction and the rates of several biochemical processes, and so these effects potentially cascade into a wide range of cellular behavior (Miermont et al., 2013; Tsai et al., 2019; Oldewurtel et al., 2019).

The nature and dynamics of how a cell responds to perturbation are complex and depend on the antibiotic class (and thus target molecule abundance, Mitosch and Bollenbach, 2014), dose (Greco et al., 1995), exposure time (Michael et al., 2016), affinity to the target molecule (Greulich et al., 2015), as well as bacterial species (Rahal and Simberkoff, 1979; Gupta, 2011), growth phase (Wood et al., 2013), rate (Tuomanen et al., 1986; Brown et al., 1990; Greulich et al., 2015), and environment (Kwon et al., 2010; Mitosch and Bollenbach, 2014). The fact that bacteria can use antibiotic molecules for signaling, for example, to coordinate multicellular processes within a population in antibiotic-induced biofilm growth (Jerman et al., 2005; Hoffman et al., 2005), exemplifies both the complexity and elegance of such responses. The multi-factorial character of bacterial responses to antibiotics brings together a number of distinct (e.g., genetic, metabolic, structural) processes impacting the cell's physiology.

However, exposure to antibiotics also perturbs the global physiological state of the cell. Exposure to an antibiotic may change the expression rate of a specific gene or gene cluster to compensate directly for the drug's action, for example by increasing the number of target protein to compensate for its inhibition or to synthesize machinery to repair antibiotic-induced damage (Lin et al., 2005; Khil and Camerini-Otero, 2002; Shaw et al., 2003). Also, through global changes to the physiology (e.g., effects on the growth rate), antibiotics alter global gene expression patterns (Mitosch and Bollenbach, 2014). The total number of

genes affected varies significantly for different antibiotics (Lin et al., 2005). Furthermore, antibiotics have been shown to affect macromolecular composition, including protein-to-DNA ratio (Bollenbach et al., 2009), and the RNAP (Klumpp and Hwa, 2008) and ribosome concentrations (Scott et al., 2010). The concentrations of other key cellular species such as second messengers (e.g., Hoffman et al., 2005) and the alarmone molecule, (p)ppGpp (Dalebroux and Swanson, 2012), were also reported to change, further contributing to global changes in gene expression.

The *E. coli* genome is several orders of magnitude longer (∼1.5 mm) than the cell length (typically 1–2 μm), and so it is tightly packaged in the cell volume (Stavans and Oppenheim, 2006; Dame, 2005). It is organized, together with RNA and proteins, into a highly compacted structure called the nucleoid. As reviewed in (Benza et al., 2012), the organization is at various scales, starting at the level of DNA strands, which interact with themselves, RNA, and the nucleoid-associated proteins (NAPs) forming bridges, bends, and loops; then at intermediate length scales, giving rise to supercoiled domains; and then globally in "macro-domains" of several million base pairs. Fluorescence microscopy of tagged genetic sites allows to probe in living cells some of these physical properties, by monitoring the fast local dynamics (fluctuations) of the chromosome (Espeli et al., 2008; Weber et al., 2010a; Javer et al., 2013; Wlodarski et al., 2017; Crozat et al., 2019). If one observes chromosome motions over time intervals longer than approximately 1 minute, they are dominated by segregation and cell growth, which will appear as super-diffusive directed (ballistic) motion (Espeli et al., 2008; Cass et al., 2016). In contrast, displacements at time intervals below 10 s are interpreted as fluctuations in a complex local environment, reflecting "microrheology" properties (Waigh, 2005; Cicuta and Donald, 2007; Wlodarski et al., 2017).

In complex viscoelastic fluids the $MSD(\tau) = \langle (\mathbf{x}(t + \tau) - \mathbf{x}(\tau))^2 \rangle$, where x is the position of a particle at a given time and the angular brackets reflect a time and/or ensemble average, is often found to follow a scaling τ^α, with the exponent $0 < \alpha < 1$ indicating sub-diffusion (for diffusion, $\alpha = 1$).

The local physical properties of the *E. coli* chromosome and cytosol have been probed in a number of experimental studies. Weber et al. first revealed that chromosomal loci move subdiffusively with a power law exponent around $\alpha \sim 0.4$. Our team also explored these motions, showing in Javer et al. that a small proportion (1%–2%) of chromosomal loci shows seemingly directed ballistic motion (Javer et al., 2014) and that in the presence of this fluorescent tag the amplitude of short time scale chromosomal motion varies for different positions along the genome, with loci located closer to the origin of replication showing larger motions compared with those closer to the terminus of replication (Javer et al., 2013). This is consistent with uneven NAP-binding sites, specifically MatP condensation (Dame et al., 2011; Espéli et al., 2012; Crozat et al., 2019), and enzyme activity distributions along the genome observed previously (Sobetzko et al., 2012).

Similarly to chromosomal loci, cytosolic tracer objects also display subdiffusive motion, with non-trivial size dependence. A recent study by Parry et al. showed that size-calibrated aggregates of cytosolic avian reovirus protein μNS, abbreviated as μNS-GFP (which are foreign to *E. coli*) display metabolism-dependent motion, with the difference in the *MSD* between metabolically active and inactive cells increasing strongly with aggregate size (Parry et al., 2014). The same study, and to date the only one, explored the effects of an antibiotic, rifampicin, on cytosol dynamics. A relatively high dose was used to switch off transcription, and this caused a small reduction of mobility in the cytosolic μNS-GFP aggregates. The study measured *MSD* for long lag times (minutes to hours) (Parry et al., 2014). In another study of crowding, hyper-osmotic shock conditions of >0.28 osmol caused a decrease in the cytosol dynamics (quantified as change in the diffusion coefficient of GFP). The change was proportional to the magnitude of the osmotic upshift (Konopka et al., 2006). It is an open question which (or both, jointly) of the chromosome or the crowded cytosol is causing the complex dynamics observed in the other. Consequently, it is valuable to measure both motions under the same cell perturbations.

In this work, we investigate response phenotypes by characterizing the effects of sub-lethal doses of clinically important antibiotics and of sorbitol (a hyperosmotic shock inducer) on short (<15 s) timescale chromosome and cytosol dynamics in *E. coli* grown in standard growth conditions on agarose pads (Figures 1A and 1B). To enable long (several hours) measurements on the same cells, as critical for investigating the effects of antibiotics, it is essential to use the data-correction method for dynamics that we developed previously (Wlodarski et al., 2017); this accounts for both marker photo-bleaching and marker size effects. We
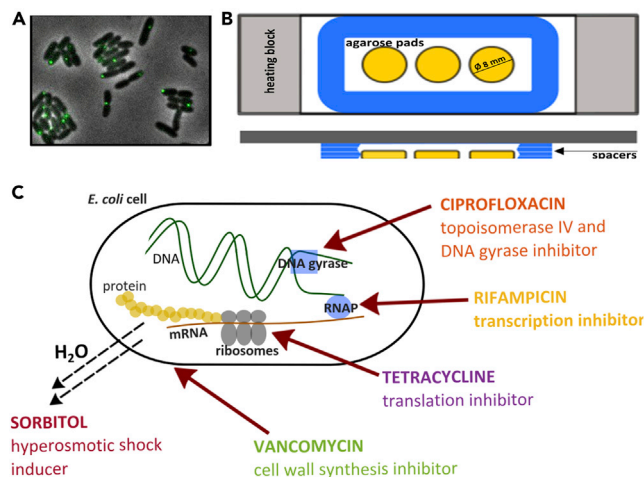
Figure 1. Experimental Approach

Chromosomal and cytosolic markers are tracked in each cell, under treatments with antibiotic and crowding agents. The trajectories are quantified through the mean square displacement (*MSD*) of the fluorescent tracer, either chromosomal or cytosolic, following the methods of Wlodarski et al. (2017). All *MSD* are well described by power laws of the time interval τ, τ^α. One expects the *MSD* amplitude to be inversely proportional to the viscoelastic resistance of the surrounding medium. Chromosomal Ori2 and Ter3 loci explore space slower than the cytosolic μNS aggregates.

(A) Example of phase contrast image of live *E. coli* cells, overlayed to the fluorescence channel showing chromosomal loci (*green*).

(B) The schematic top and side views show how the samples are contained for live imaging: agarose pads (*yellow*) are sealed between a coverslip and a glass slide with spacers (*blue*) and sit on a heating block (*gray*) for temperature control.

(C) We explore sub-lethal doses of four antibiotics, chosen from four major antibiotic classes, and a hyperosmotic shock-inducing agent, sorbitol. The antibiotics are chosen to have very different targets: DNA replication (ciprofloxacin), transcription (ciprofloxacin and rifampicin), translation (tetracycline and chloramphenicol), and cell wall synthesis inhibitors (vancomycin).

find that most tested treatments cause small effects on mobility, coherently for both chromosomal loci and cytosolic aggregates. We also find that different antibiotics have different effects on genome and cytosol dynamics. We then investigate the mechanistic reasons behind the observed changes in intracellular mobility under antibiotic treatments by assaying macromolecular crowding. As a measure of global crowding we assay cell density using optical readings and estimations of dry mass and refractive index (RI). Our results show a previously unknown robust correlation between the mobility of genetic material and of cytoplasmic particles and intracellular density in the presence of antibiotics.

RESULTS

Sub-lethal Antibiotic Treatments Cause Small but Consistent Effects on Genome and Cytosol Dynamics

For an initial comparison of mobility across the effects of treatments we choose the *MSD* at an (arbitrary) lag time of 10 s (τ = 10 s). The results show that in untreated bacteria, mobilities of both chromosomal loci and cytosolic μNS aggregates remain fairly stable throughout the experiments (Figure 2, blue lines on all panels). As expected, the cytosolic aggregates show higher mobilities (*MSD*(10s) $\simeq$ 0.08 μm^2), whereas chromosomal loci show *MSD*s of an order of magnitude lower at 10-s lags, with Ori2 loci exploring space faster than Ter3 loci (*MSD*(10s) $\simeq$ 4.0×10^{-3} and $\simeq$2.5×10^{-3} μm^2, respectively).

Bacteria were all first grown in identical conditions (seeMethods), and then delivered on agar pads containing different antibiotics or sorbitol. Antibiotic experiments were performed at sub-lethal doses ($\sim$75% of the minimal inhibitory concentrations [MIC]), determined for each tested strain using a standard agar dilution MIC determination method (Wiegand et al., 2008) (see Methods for details). The bacteria were observed repeatedly for up to 2 h (T_{treat} = 20–120 min), under treatment with four clinically important antibiotics of distinct classes (and thus different modes of primary action): ciprofloxacin (type II topoisomerase inhibitor), rifampicin (transcription inhibitor), tetracycline (translation inhibitor), and vancomycin (cell
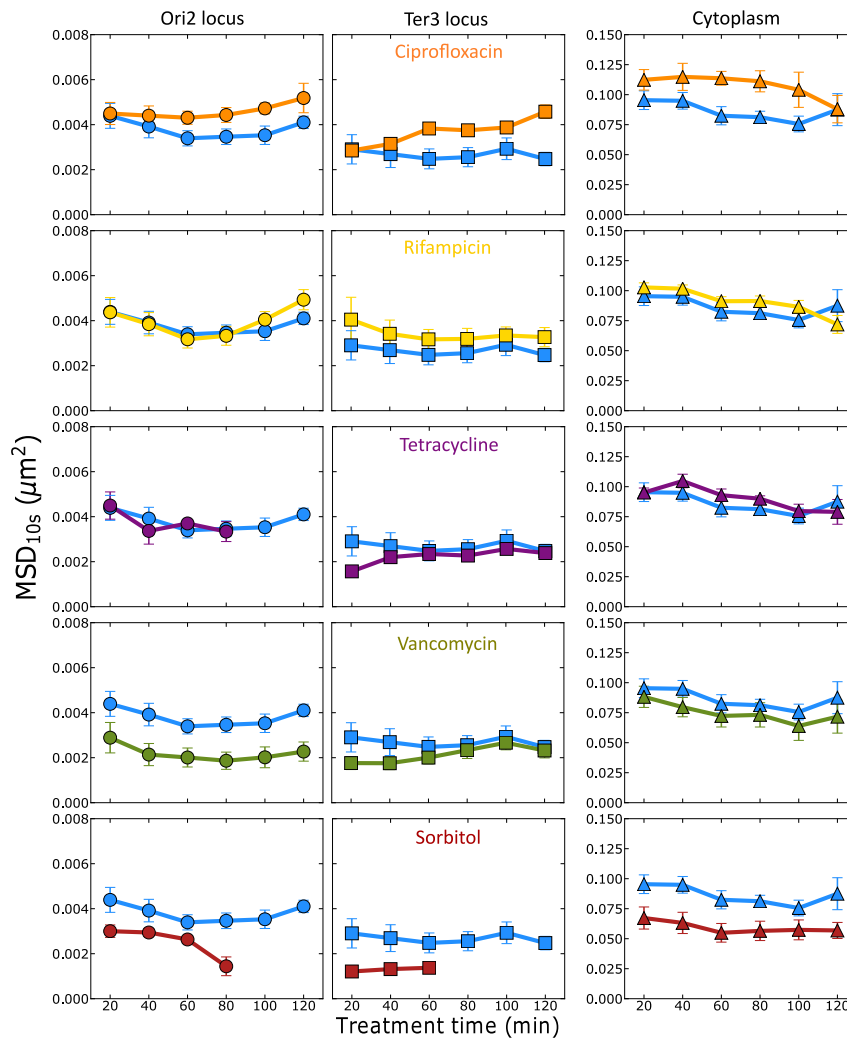
Figure 2. Sub-lethal Antibiotics and Sorbitol Change the Mobility of Both Chromosome and Cytosol

There are small but consistent changes to the short timescale mobility MSD(10 s) over treatment time (T_{treat} = 20–120 min) for different antibiotics and sorbitol (in different colors as indicated in the figure), compared with control (*blue* lines) for the marker at the Ori2 locus (*circles*), the Ter3 locus (*squares*), and for the cytoplasmic particle (*triangles*). Data points show the average of the medians from 9 (chromosomal loci) and 6 (particles in cytoplasm) independent replicates. Error bars show the standard error. p Values are given in Table S2 and Supplemental Information.

wall synthesis inhibitor) as illustrated in Figure 1C. In addition, bacteria were grown on an agar pad with 400 mM sorbitol, capable of inducing a hyperosmotic shock in *E. coli* as reported previously (Rojas et al., 2014). Overall, nearly 100,000 chromosome loci tracks were collected across all treatment conditions and measurement times (refer to Table S1 and Supplemental Information for details).

We find that sub-lethal doses of most of the tested antibiotics and sorbitol cause small changes to short timescale (10-s lags) dynamics of both chromosomal loci and cytosolic μNS aggregates (Figure 2). Importantly, the effects are consistent between the three markers and, in most cases, over the entire drug exposure time.

Treatment with ciprofloxacin increases the MSD of both Ori2 and Ter3 loci gradually over the treatment time, up to $\simeq 4.0 \times 10^{-3}$ and $\simeq 2.5 \times 10^{-3}$ μm^2 at the final treatment time point (T_{treat} = 120 min), respectively. Cytosolic μNS aggregates show an increased MSD already at the initial time point (T_{treat} =

20 min) and gradually decrease mobility and reach the control level ($\simeq 0.08$ μm^2) at the final treatment time point.

We observe a similar trend for rifampicin, as reported by us recently (Wlodarski et al., 2017). This is a smaller effect than with ciprofloxacin, and especially minute for the Ori2 locus, whose mobility increases up to $\simeq 5.0 \times 10^{-3}$ μm^2 only for $T_{treat} > 90$ min. Ter3 mobility remains increased fractionally, but consistently, to the level of $\simeq 3.5 \times 10^{-3}$ μm^2 across the whole drug exposure time. Effects are also very small for cytosolic μNS aggregates, whose MSD remains higher by ~ 0.01 μm^2 throughout the whole treatment time, except for the final time point.

Tetracycline is the only treatment agent tested in this work that does not show consistent effects on the mobility of the three markers. In addition, as translation inhibition causes a decrease in ΔParB-GFP production, the lower amount of fluorescent protein allows photo-bleaching to make all trackable Ori2 loci disappear after 80 min of experiment.

Vancomycin causes a small decrease in MSD of both chromosomal loci already at the initial treatment time point ($\simeq 3.0 \times 10^{-3}$ and $\simeq 2.0 \times 10^{-3}$ μm^2 for Ori2 and Ter3 loci, respectively) and continues to decrease Ori2 loci mobility down to $\simeq 2.0 \times 10^{-3}$ μm^2, whereas Ter3 mobility loci remains relatively constant. Mobility of cytosolic μNS aggregates deceases by $\simeq 0.01$ μm^2 and remains at this level till the end of the experiment. In addition, we observed that vancomycin affected visibly cell morphology causing characteristic bending of cells (Figure S9 and Supplemental Information).

Sorbitol also decreases the MSD of both Ori2 and Ter3 loci already at the initial treatment time point (about 20 min into the exposure to sorbitol). Mobility is down to $\simeq 1.5 \times 10^{-3}$ μm^2 for both Ori2 and Ter3 loci at final treatment times. Under hyperosmotic shock conditions, and likely also in cells recovered from the shock, gene expression processes may be impaired (van den Berg et al., 2017), resulting in strong marker photo-bleaching and thus inability to collect valid loci tracks after T_{treat}=80 and 60 min for Ori2 and Ter3 loci, respectively. Motility of cytosolic μNS aggregates remains decreased at $\simeq 0.06$ μm^2.

We also observed changes to the scaling exponent α, a result reported recently by Yu et al. (2018) in mechanically compressed *E. coli* cells. The antibiotic-induced changes to α observed in this work are much smaller (changes of up to 16% at the shortest T_{treat}, Figure S3) compared with those in compressed cells (change of at least 20% at 20 psi for all markers).
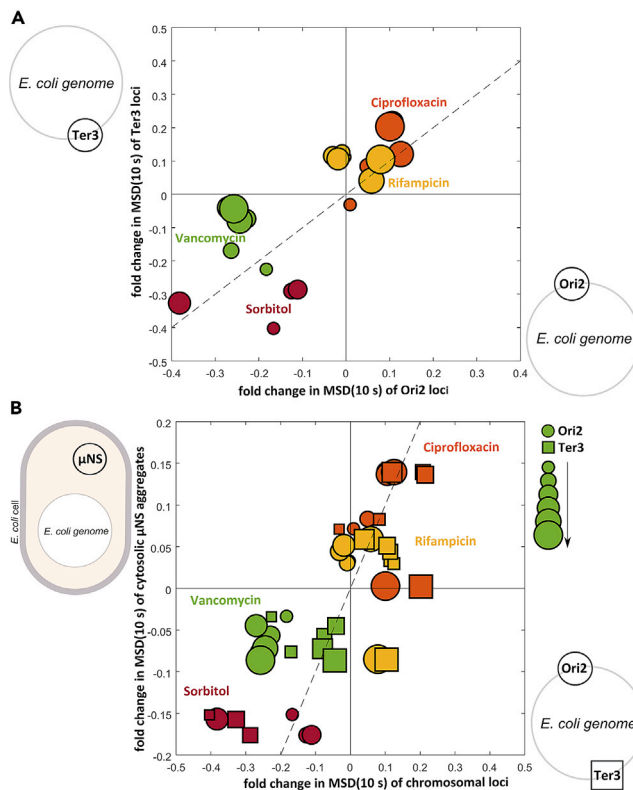
Directions of Effects Generally Correlate between Chromosomal Ori2 and Ter3 Loci

To compare chromosomal responses directly, we considered relative fold changes in mobility, defined as the logarithm of treated-to-control MSD(10 s) ratios, for Ori2 and Ter3 loci for individual treatments and treatment times (Figure 3A). The directions of these effects are consistent for the Ori2 and Ter3 chromosomal loci for each of the treatment conditions.

Notably, the initially fast-moving loci, Ori2, increased their mobility less when treated with ciprofloxacin and rifampicin (maximal fold changes +0.12 and +0.08, respectively) when compared with the initially slow-moving loci, Ter3 (maximal fold changes +0.2 and +0.1, respectively). Conversely, the initially slow-moving loci, Ter3, decreased their mobility less when treated with vancomycin (maximal fold change −0.18) when compared with the initially fast-moving loci, Ori2 (maximal fold change −0.28), and showed comparable magnitude in fold change under sorbitol treatment (maximal fold change −0.39 and −0.40 for Ori2 and Ter3, respectively).

Directions of Chromosomal and Cytosolic Effects Generally Correlate

We can also compare chromosomal and cytosolic responses directly (Figure 3B) considering relative changes in mobility defined again as the logarithm of treated-to-control MSD(10 s) ratios for chromosomal Ori2 and Ter3 loci and cytosolic μNS aggregates for individual treatments and treatment times. The directions of responses are generally consistent between chromosomal and cytosolic markers and the magnitude of fold change for chromosome and cytosol dynamics is generally comparable. In fact, most of the responses lie on or near a straight line with gradient equal to unity (Figure 3B, dashed diagonal line). This suggests that changes to the physical properties of cytosol generally correlate both in timing and magnitude with changes to the physical properties of the chromosome. Exceptions to this

Figure 3. Changes Are Generally Consistent across the Chromosome, and in the Cytosol

(A) Directions of effects generally correlate (except for vancomycin) between the chromosomal Ori2 and Ter3 loci. Fold changes in Ori2 versus Ter3 loci mobility, defined as the logarithm of treated-to-control MSD(10 s) ratios, are plotted for different treatments (in different colors as indicated in the figure).

(B) Direction of effects generally correlates also across chromosomal loci and cytosolic μNS aggregates. Fold changes in chromosomal Ori2 (*circles*) and Ter3 (*squares*) loci versus cytosolic μNS aggregates' mobility, defined as the logarithm of treated-to-control MSD(10 s) ratios, are plotted for different treatments (in different colors as indicated in the figure). Plot marker size increases with increasing treatment time (T_{treat} = 20–120 min). Diagonal dashed lines in both panels represent gradients of unity.

pattern are the Ori2 loci under vancomycin treatment, and both the chromosomal loci under the sorbitol treatment.

Detailed Chromosomal Dynamics

We also looked at how dynamics responses evolve as a function of lag time; fold changes in mobility as shown earlier for three arbitrary lag times (τ=0.1, 1.0, and 14 s) are plotted in Figure 4. The differences in responses between all tested antibiotics become apparent for τ>10 s, with data points for individual treatment conditions forming distinct clouds, especially at longer treatment times. In addition, the difference between the Ori2 and Ter3 response to vancomycin becomes well differentiated only for τ>5 s and, for ciprofloxacin and rifampicin, only at longer (T_{treat}>40 min) treatment times. Remarkably, sorbitol follows a different pattern, causing distinct effects for both chromosomal and cytosolic makers already at the shortest tested lag time (τ=0.1 s). In addition, the difference between the Ori2 and Ter3 response is apparent already at this lag time and becomes less pronounced but still distinguishable at longer lag times. We compared step-size distributions at τ=0.1 s for control (not treated) and sorbitol-treated samples and observed no significant differences (Figure S2).

Changes in the Dynamics Are Generally Consistent with Intracellular Crowding

We reasoned that as the chromosomal and cytosolic dynamics change proportionally with each other, they are possibly determined by a common factor, and that the changes to the intracellular crowding levels
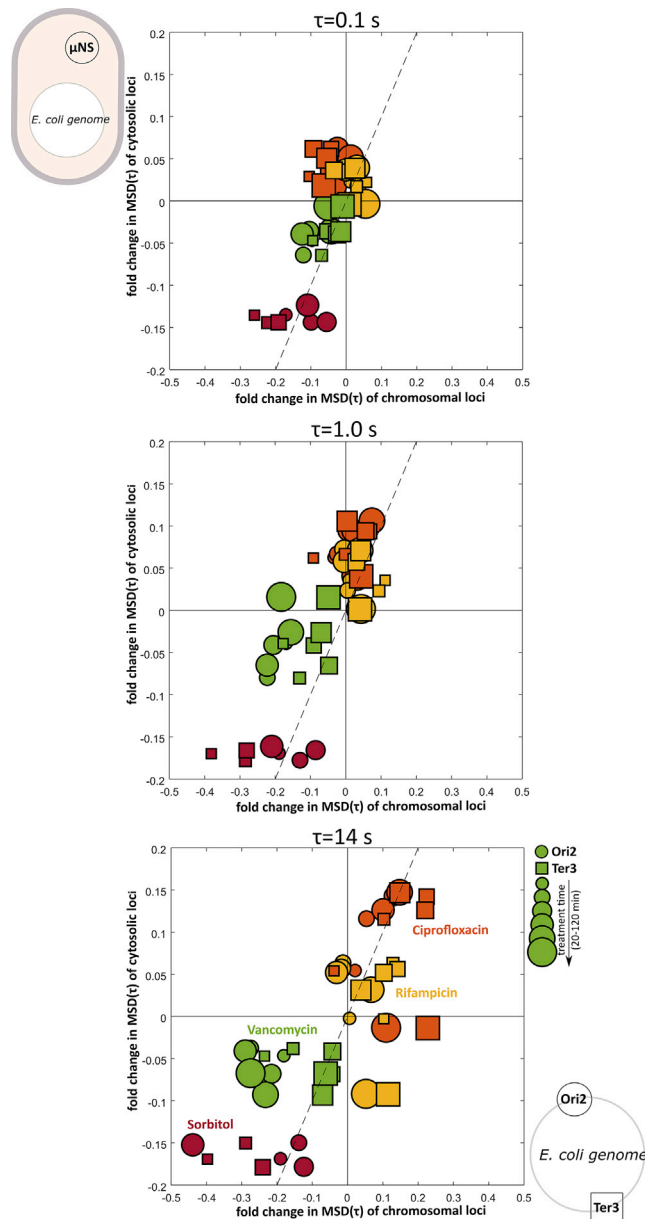
Figure 4. Dynamic Changes with Different Antibiotics and Sorbitol Depend on the Lag Time

Fold changes in chromosomal Ori2 (*circles*) and Ter3 (*squares*) loci versus cytosolic μNS aggregates' mobility, defined as the logarithm of treated-to-control $MSD(10\,s)$ ratios, are plotted for different treatments (in different colors as indicated in the figure) for three lag times (τ=0.1, 1.0, and 14 s) representing a range of tested lag times as indicated above individual figures. Plot marker size increases with increasing treatment time (T_{treat} = 20–120 min). Diagonal dashed lines represent gradient of unity.

could be an explanation. Having observed cell size changes during treatment that qualitatively recapitulated the trends observed in Figures 4A and 4B (see also Figure S4 and Supplemental Information), we speculated that if cellular mass did not follow the same trends, treated cells might have undergone changes in intracellular density and therefore in crowding levels. In single scattering regimes, that is when cells are sufficiently diluted (Stevenson et al., 2016), OD_{600} linearly correlates with the dry mass of cells (Basan et al., 2015a) (Figure S11 and Supplemental Information). As *E. coli* is thought to robustly maintain a constant density across a range of growth conditions and across cell volumes spanning half an order of magnitude (Basan et al., 2015a; Oldewurtel et al., 2019), the relationship between dry mass and OD_{600}

remains constant independent of cell size. Although OD_{600} is often considered a synonym of cell number, this is only true for cells with constant cell sizes. As a proxy for intracellular cell density we therefore assayed the relationship between OD_{600} and dry mass in both treated and untreated cells. In contrast to what was observed for cells grown for many generations in constant non-limiting conditions (i.e., steady state) (Basan et al., 2015a), cells treated with sub-lethal concentrations of ciprofloxacin or rifampicin for 1 h exhibited a biomass to OD_{600} ratio 10% lower than that of untreated cells. We observed even more significant changes in the case of sorbitol, although in the opposite direction, with cells showing a biomass-to-OD_{600} ratio larger by about 30% than untreated cells. Our values for untreated cells are overall in agreement with those previously reported in the literature (Ren et al., 2013; Long et al., 2016; Folsom et al., 2014; Basan et al., 2015b; Stevenson et al., 2016).

We then reasoned that the washes necessary for estimating dry mass could potentially cause a certain level of cell lysis to which antibiotic-treated cells may be more susceptible. We tested this by monitoring optical density (OD) after repeated washes finding no sign of lysis (Figure S11B and Supplemental information). We also considered that some cell growth might take place during sample handling. Although in our work antibiotics are used at a sub-inhibitory concentration, they could still slow down the growth rate of treated cells, thereby introducing artifacts in our dry mass measurements. Thus we repeated our measurements by carrying out all the sample handling on ice, obtaining results that are in line with those obtained when the handling was performed at room temperature (Figure S11C and Supplemental Information). (We note that ice could in turn introduce artifacts by altering cell physiology, for example, by inducing the cold shock response). We further reasoned that the changes observed could have also been explained by changes in the RI of the treated cells, which would have influenced the OD readings. OD indeed scales with the ratio between the RI of the cells and the one of the medium, reaching zero OD when the two match (Marquis, 1973; Bateman et al., 1966). We took advantage of this relation to estimate the RI of cells across our treatment conditions. We progressively added BSA, which alters the medium's RI in a known way (Barer and Tkaczyk, 1954; Crespi et al., 2012) (Figure 5B, inset), to cell suspensions until OD became zero. The RI of the BSA solution in which cells had zero OD was therefore equal to the RI of our cells. As suspensions of treated and untreated cells lost OD at similar BSA concentration, we concluded that their RI was not varying significantly and that our biomass-to-OD_{600} values can be interpreted as changes in density.

The changes in density, and thus of crowding levels, caused by the treatments were generally consistent with those observed in the loci and cytoplasmic mobility (Figure 5C) with the exception of vancomycin, which instead showed no correlation. As the antibiotics used in our treatments target different cellular functions, we wondered whether the changes in density were accompanied by changes in macromolecular composition. Given that protein is the most abundant molecular species of the bacterial cell (Bremer and Dennis, 2008), we assayed cells' protein content via two independent colorimetry assays: the Bradford and Biuret assays. Our assays report protein levels for untreated cells that are in good agreement with the literature (You et al., 2013) and did not show any significant change in the relative protein content after treating cells for 1 h with antibiotics or sorbitol, except perhaps a small increase in the case of rifampicin treatment (Figure 5C). Taken together, these findings show that under certain antibiotic treatments (ciprofloxacin and rifampicin) and in certain environmental conditions (hyperosmotic shock), bacteria temporarily lose the ability of regulating their cell density, albeit, at least from the point of view of protein, maintaining the capability of keeping a certain level of control upon the relative abundance of their macromolecular components.

DISCUSSION

The Fast Dynamics of Genome and Cytosol at Long (Several Hours) Drug Exposure Times

Many important aspects of how antibiotics affect bacterial physiology remain unknown. Our current challenge is to provide a more holistic picture of antibiotic effects. For example, this question has been approached through DNA microarray studies on global gene expression (Lin et al., 2005). However systems-level physiological responses such as effects on gene regulatory networks and on the macromolecular composition of cells (e.g., the concentration of ribosomes and protein-DNA ratio) remain largely unexplored. Our study provides a complementary viewpoint on the response phenotypes of different antibiotics.

The data treatment procedure we developed (Wlodarski et al., 2017) measures long-term (several hours) changes to marker dynamics, accounting for marker photo-bleaching and marker size effects. These
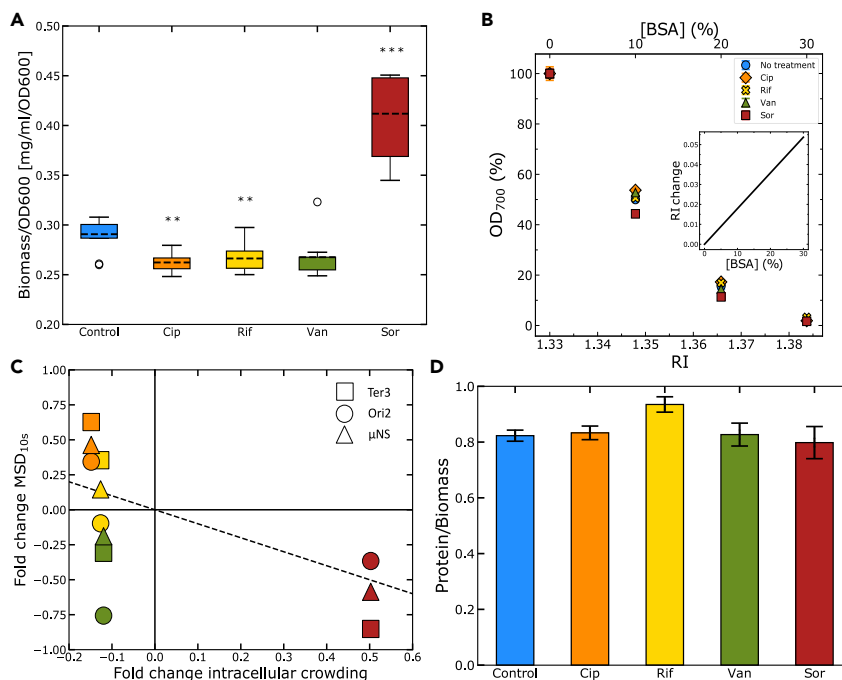
Figure 5. Changes in Cytosol Crowding Levels Are Consistent with Effects on Intracellular Dynamics

(A) Biomass to OD_{600} ratio of cells after 1 h of antibiotic treatment. Treatment conditions include: Control (not treated); Cip, ciprofloxacin; Rif, rifampicin; Van, vancomycin; and Sor, sorbitol. Data for each condition were obtained from three biological replicates, performed in triplicates. Statistical significance of the differences with the untreated control was assayed via a t test, obtaining the following p values: Cip, 0.002; Rif, 0.008; Van, 0.052; Sor, 0.0001.

(B) Refractive index (RI) of cells measured by comparing with the RI of BSA solutions. Inset: RI change due to dissolved BSA.

(C) Scatterplot of the $\log_2$ of fold change in MSD(10 s) after 1 h of treatment versus fold change in crowding levels under the four treatments. The dashed diagonal line represents a gradient of negative unity.

(D) Protein contribution to the total biomass for treated and untreated cells. <u>Error bars show the</u> standard error. Error propagation of the error was carried out according to the formula: $SE_{a/b} = \sqrt{(SE_a/A)^2 + (SE_b/B)^2}$ where SE_a and SE_b are the standard errors of protein and biomass and A and B are their respective means. Protein quantification data from five biological replicates performed in triplicates with two independent methods. Statistical significance of the changes compared with the control was tested with a t test obtaining the following p values: Cip, 0.917; Rif, 0.267; Van, 0.968; Sor, 0.794.

corrections enable investigation of long-term responses to antibiotics, which commonly can cause gradual and cumulative changes to the expression levels of a large number of genes (Lin et al., 2005; Khil and Camerini-Otero, 2002; Shaw et al., 2003) as well as evolutionary adaptations often taking place over tens of generations (Michael et al., 2016). Some of the previous studies on genome and cytosol dynamics included insights on the effects of antibiotic treatments (Weber et al., 2010a; 2012; Parry et al., 2014); however, they did not consider these corrections. In addition, these studies were limited to single time point dynamics measurements and to high (above estimated IC_{50}) antibiotic doses (e.g., Weber et al., 2010a; Parry et al., 2014). Addressing these points reveals with higher precision that sub-lethal antibiotic and sorbitol treatments have small but consistent effects on genome and cytosol short timescale mobility.

Genomic Position Affects the Degree of Response

We observe that almost all tested antibiotics (with the exception of tetracycline) cause changes to the chromosome dynamics and that these changes persist for most of the treatment time. We also show that the directions of effect are generally consistent for both Ori2 and Ter3 loci. Notably, we show that the change in the amplitude of motion depends on the initial locus mobility (before treatment). The initially fast-moving loci, Ori2, increase their mobility less when treated with ciprofloxacin and rifampicin when compared with the initially slow-moving loci, Ter3. The opposite is true for vancomycin.

The amplitude of these local motions may measure factors such as the level of genetic locus "compaction" and the macromolecular crowding of the cytosol, respectively (Weber et al., 2010a; Javer et al., 2013). Consequently, limitations to changes in motion may suggest a functional limit to maximal relaxation and compaction of a genetic locus and the ability of a bacterial cell to alter the genome's physical environment flexibly, not only depending on external stimuli but also on the chromosomal coordinate of a gene. Possible reasons for such limits include heterogeneity of the intracellular medium, of locus-specific NAP density, of locus confinement, and the physical state of the DNA molecule (torsion, elasticity, etc.).

Deviations from "Polymer in Viscoelastic Cytosol" Model of Chromosome Dynamics Are Only Mild

Beyond the specificities, which demand future investigations, most of the responses, when plotted as fold changes in chromosomal against cytosolic mobility, lie around a straight line with slope equal to unity (Figure 3B). This general correlation in both timing and magnitude of responses between the chromosome and cytosol is overall consistent with the physical representation of the chromosome as a "polymer embedded in a viscoelastic medium" (Lampo et al., 2016; Weber et al., 2010b; Polovnikov et al., 2018). In this model, individual parts (e.g., genetic loci) of such polymer explore space by sub-diffusing through a crowded environment of macromolecules, some of which (e.g., nucleic acids and cytoskeletal filaments) possess significant elastic properties. It follows that changes to the viscosity of the surrounding medium will affect the energy states of individual polymer parts (Weber et al., 2010b; Benza et al., 2012; Bakshi et al., 2014). Consequently, we speculate that the treatment-induced chromosomal effects are a direct physical consequence of changes in the concentration of the cytosol.

We recently reported a violation of the predictions of the polymer in viscoelastic fluid model for the intracellular dynamics *immediately* after cells were compressed mechanically (Yu et al., 2018). This violation was proxied by a change in the ratio of the scaling exponents of cytoplasmic particles and chromosomal loci. Such deviation is probably due to the fact that the chromosome is not fully embedded in the cytoplasm, but is, at least in part, a separate "compartment," consistent with the observation that the nucleoid has a different density to the cytoplasm (Valkenburg and Woldringh, 1984). A similar deviation is observed in this study (which also has slightly lower precision than the previous one), but it is quantitatively smaller (10%–16% instead of more than 20%, see Figure S3). We believe that this is likely because in this case the system has more time to equilibrate after the perturbation, as the measurements are performed more than 20 min after the perturbation. Possibly a differential role of osmotic forces from ribosomes in the presence of certain antibiotics may also play a role (Bakshi et al., 2014).

Antibiotic-Induced Changes in Crowding Affect the Cell Globally

Should the observed chromosomal dynamics effects be a consequence of changes to the properties of the cytosol, it is the cytosolic macromolecular crowding that would mediate these effects. This would be a direct consequence of the fact that as the cytosol becomes more crowded, larger structures such as the chromosome cannot diffuse freely due to significant steric hindrance. Increased depletion-attraction interactions between crowded macromolecules may also cause the chromosome material to reduce its size for other molecules to have more space and relieve steric constraints.

Our measurements of cellular density suggest that indeed the mobility of both chromosomal and cytosolic markers is generally inversely proportional to the crowding level (Figure 5C). This finding suggests that the previously reported widespread genetic effects of antibiotics can at least partially be a consequence of antibiotics altering the nucleoprotein microenvironments of genetic loci via effects on the crowding levels.

Sophisticated mechanisms of regulation of many important cellular parameters through macromolecular crowding may be very widespread. For example, Joyner et al. (2016) have recently reported that dramatic changes to the macromolecular crowding levels in both bacteria and yeast are part of the response to glucose starvation conditions. In this context, the increase in the crowding level is thought to be a consequence of cell volume reduction and serves as a mechanism to reduce diffusional mobility and achieve homeostasis during environmental stress. More recently, Delarue et al. (2018) showed that changes in the crowding levels can be a consequence of the mTORC1 signaling pathway effects on the ribosome concentration. Using cytosolic particles of tunable size, the authors showed that macromolecule (ribosome) concentration can exert particle size-dependent effects on molecular diffusivity, opening a possibility to differentially modulate cellular reaction rates depending on particle size.

Antibiotic-Specific Responses in Cell Concentration

Based on the aforementioned considerations, we can attempt to rationalize the antibiotic-specific effects that we have observed. For ciprofloxacin, it is plausible that the observed dynamics effects are caused primarily through inhibition of topoisomerase IV, an *E. coli* quinolone target secondary to DNA gyrase. Interference with decatenation of replicated DNA strands causes excessive cell filamentation and significant dilution of cytosol contents. The latter is likely to result in an increase in cytosolic aggregate and chromosomal loci mobility. Work of Weber et al. (2010a; 2012) also points to the causal role of topoisomerase IV. In their work novobiocin, an aminocoumarin antibiotic that similar to ciprofloxacin targets DNA gyrase but has a significantly lower affinity to topoisomerase IV (Hardy and Cozzarelli, 2003), caused no significant change to loci mobility.

Our rifampicin effects are generally consistent with those reported by Weber et al., who showed that after longer (≥ 5 but ≤ 30 min) treatments, chromosomal loci mobility increased and plateaued at an approximately 2-fold greater magnitude (Weber et al., 2012). Although Parry et al. (2014) reported a small decrease in the mobility of cytosolic µNS aggregates under rifampicin treatment, the tested dose was high enough (25 µg/mL, 1.5× expected MIC) to likely cause severe changes to cell physiology (e.g., near-complete shutdown of gene expression and significant growth stalling). Following Weber et al. (2012) and Bakshi et al. (2014), we propose that RNAP inhibition and mRNA pool decay, combined with subsequent ribosomal subunit-nucleoid mixing, cause a decrease in cytosol viscosity and nucleoid expansion, ultimately increasing cytosolic µNS aggregate and chromosomal loci mobility.

Interestingly, the same study reported that treatment with chloramphenicol, a protein synthesis inhibitor that (similar to tetracycline) targets the 30S ribosomal subunit to stall translation, resulted in an increase in chromosomal loci mobility. This is not consistent with our finding that tetracycline causes no consistent effect on loci mobility. However, the chloramphenicol dose used by Weber et al. (25 µg/mL, 2,500× expected MIC) was much higher than our tetracycline dose. We observed that while tetracycline was the only treatment agent that affected (and decreased) cell lengths (Figures S4 and S6 and Supplemental Information) (and also elongation rates, Figures S5 and S7 and Supplemental Information), it also increased cell widths (Figure S8 and Supplemental Information). It seems that these two changes to cell size canceled out resulting in no net change to cytosol viscosity. It is possible that responses to different doses could be different. It would also be particularly useful to establish and test a tetracycline dose that does not affect cell elongation rates as was achieved for all other treatments in this work.

For vancomycin, although we detected only very small and not consistent effects on cell lengths and elongation rates (Figures S5 and S7 and Supplemental Information), we noticed significant changes to cell morphology such as bending of cells (Figure S9 and Supplemental Information). Inhibited cell wall synthesis resulted in impaired cell elongation and thus morphological defects, possibly creating conditions for condensation of cell contents and reduced mobility of tracked markers.

For sorbitol, at least in the case of the strain harboring the marker at the Ori3 locus, our cell size measurements show a progressive volume recovery through our treatment time (Figure S5 and Supplemental Information). Examining such recovered cells with fluorescence recovery after photobleaching (FRAP), Konopka et al. observed an ~2-fold decrease in the GFP diffusion coefficient and an ~2-fold increase in the biopolymer volume fraction (cytoplasmic volume occupied by biopolymers such as proteins and the nucleoid) compared with pre-shock cells (Konopka et al., 2009). Our results are in general agreement with these measurements as we observed a nearly 2-fold decrease in the *MSD* of cytosolic µNS aggregates and an ~1.3 fold increase in the macromolecular crowding level. Such changes are likely due to the intrinsic rigidity of the cell wall/outer membrane system (Rojas et al., 2018). In post-hyperosmotic shock cells, an increase in crowding is likely also due to the increased intake of osmolites during the recovery (Wood, 2006). Regarding our inability to collect valid tracks of chromosomal markers after 60–80 min of experiment, it is likely that the hyperosmotic shock conditions impaired the production of ΔParB-GFP proteins, and that some of that impairment persisted also in the recovered cells—for example, as a consequence of the increased crowding discussed earlier. Cytosolic µNS aggregates (which assembled before the shock) appeared stable throughout the experiments.

As the change in the cytosolic density is common to all proposed mechanisms and it underpins the changes to cytosolic and chromosomal dynamics, we surmise that the crowding level is the key driver of the

observed dynamics. At the same time, we hypothesize that other factors—such as local differences in folded organization of the chromosome, the distributions of NAP and enzyme binding sites, etc.—contribute to the deviation from the general linear correlation between both cytosolic and chromosomal dynamics (Figure 3) and between the crowding level and marker mobility (Figure 5).

Conclusions

By performing high-throughput and high-precision intracellular marker tracking, we discovered that sub-lethal doses of ciprofloxacin, rifampicin, and vancomycin as well as hyperosmotic shock conditions caused small but consistent changes (unique to each treatment agent) to the physical organization of chromosomal Ori2 and Ter3 loci and the cytosol. Crucially, there are strong correlations between the effects in different parts of the chromosome and between the chromosome and cytosol. Comparison of intracellular protein density under the treatments and of the magnitude of treatment-induced changes to the crowding levels lead us to the conclusion that mobility of both chromosomal and cytosolic markers is generally inversely proportional to the crowding level. We conclude that antibiotics, by affecting the macromolecular composition of the cell, can alter the physical microenvironments of the genome and the biosynthetic machinery, potentially affecting expression levels of a large number of genes.

Based on our findings, we propose specific mechanisms—consistent with known modes of action and with the current physical view of the bacterial chromosome and cytoplasm—on how different antibiotics can exert their effects. In brief, our results show that the main physical chromosomal and cytosolic responses to a wide range of sub-lethal treatments can be interpreted in the context of intracellular crowding. In this framework, we speculate that these mechanisms could contribute to switch, or tip, crowding homeostasis (van den Berg et al., 2017), in a way that is qualitatively generic to any antibiotic treatment or stress, but quantitatively specific to each perturbation. Crowding could itself affect growth (Klumpp and Hwa, 2014; Scott et al., 2014), thus affecting fitness changes even at mild levels of perturbations. We are just beginning to reveal this interplay between physical degrees of freedom and the global state of a cell, and indeed there is one experiment in our study, the motilities after perturbation with vancomycin, which is not explainable as a simple consequence of crowding.

Limitations of the Study

Our work portrays changes in intracellular motility and molecular crowding due to antibiotic treatment, but does not delve on the mechanisms through which these come to be. Our measurements of cellular density were carried out at the population level, therefore requiring a certain amount of handling of the samples, which could introduce experimental errors. Although we tried to exclude possible sources of artifactual nature with our controls, investigations of crowding at the single-cell level, which we could not pursue due to a lack of tools, would be an interesting way to confirm our population-level findings, particularly for the cases of rifampicin and vancomycin treatments in which biomass to OD changes are smaller.

Resource Availability

Lead Contact

Pietro Cicuta pc245@cam.ac.uk.

Materials Availability

Further information including reasonable requests for materials should be directed to and will be fulfilled by the Lead Contact, pc245@cam.ac.uk.

Data and Code Availability

The code is available from https://github.com/ver228/bacteria-loci-tracker and data are available from 10.5281/zenodo.3836129.

METHODS

All methods can be found in the accompanying Transparent Methods supplemental file.

SUPPLEMENTAL INFORMATION

Supplemental Information can be found online at https://doi.org/10.1016/j.isci.2020.101560.

AUTHOR CONTRIBUTIONS

M.W., L.M., and P.C. conceived the experiments. M.W., B.R., and L.M. performed experiments. M.W., L.M., and B.R. analyzed data. M.W., L.M., B.S., M.C.L., and P.C. wrote the paper.

DECLARATION OF INTERESTS

None declared.

REFERENCES

Bakshi, S., Choi, H., Mondal, J., and Weisshaar, J.C. (2014). Time-dependent effects of transcription- and translation-halting drugs on the spatial distributions of the E. coli chromosome and ribosomes. Mol. Microbiol. 94, 871–887.

Barer, R., and Tkaczyk, S. (1954). Refractive index of concentrated protein solutions. Nature 173, 821–822.

Basan, M., Hui, S., Okano, H., Zhang, Z., Shen, Y., Williamson, J.R., and Hwa, T. (2015a). Overflow metabolism in escherichia coli results from efficient proteome allocation. Nature 528, 99–104.

Basan, M., Zhu, M., Dai, X., Warren, M., Sévin, D., Wang, Y.P., and Hwa, T. (2015b). Inflating bacterial cells by increased protein synthesis. Mol. Sys. Biol. 11, 836.

Bateman, J.B., Wagman, J., and Carstensen, E.L. (1966). Refraction and absorption of light in bacterial suspensions. Kolloid-Zeitschrift Z. für Polymere 208, 44–58.

Benza, V.G., Bassetti, B., Dorfman, K.D., Scolari, V.F., Bromek, K., Cicuta, P., and Lagomarsino, M.C. (2012). Physical descriptions of the bacterial nucleoid at large scales, and their biological implications. Rep. Prog. Phys. 75.

van den Berg, J., Boersma, A.J., and Poolman, B. (2017). Microorganisms maintain crowding homeostasis. Nat. Rev. Microbiol. 15, 309–318.

Bollenbach, T., Quan, S., Chait, R., and Kishony, R. (2009). Nonoptimal microbial response to antibiotics underlies Suppressive drug interactions. Cell 139, 707–718.

Bremer, H., and Dennis, P.P. (2008). Modulation of chemical composition and other parameters of the cell at different exponential growth rates. EcoSal Plus 1, 1.

Brown, M.R., Collier, P.J., and Gilbert, P. (1990). Influence of growth rate on susceptibility to

antimicrobial agents: modification of the cell envelope and batch and continuous culture studies. Antimicrob. Agents Chemother. 34, 1623–1628.

Cass, J.A., Kuwada, N.J., Traxler, B., and Wiggins, P.A. (2016). Escherichia coli chromosomal loci segregate from midcell with universal dynamics. Biophys. J. 110, 2597–2609.

Cicuta, P., and Donald, A.M. (2007). Microrheology: a review of the method and applications. Soft Matter 3, 1449.

Crespi, A., Lobino, M., Matthews, J.C.F., Politi, A., Neal, C.R., Ramponi, R., Osellame, R., and O'Brien, J.L. (2012). Measuring protein concentration with entangled photons. Appl. Phys. Lett. 100, 233704.

Crozat, E., Tardin, C., Salhi, M., Rousseau, P., Lablaine, A., Bertoni, T., Holcman, D., Sclavi, B., Cicuta, P., and Cornet, F. (2019). Multiple activities of the matp protein are involved in post-replicative pairing of sister chromosomes in escherichia coli. bioRxiv. . https://www.biorxiv.org/content/early/2019/09/04/755397. https://www.biorxiv.org/content/early/2019/09/04/755397.full.pdf.arXiv. https://doi.org/10.1101/755397.

Dalebroux, Z.D., and Swanson, M.S. (2012). ppGpp: magic beyond RNA polymerase. Nat. Rev. Microbiol. 10, 203–212.

Dame, R.T. (2005). The role of nucleoid-associated proteins in the organization and compaction of bacterial chromatin. Mol. Microbiol. 56, 858–870.

Dame, R.T., Kalmykowa, O.J., and Grainger, D.C. (2011). Chromosomal macrodomains and associated proteins: implications for DNA organization and replication in gram negative bacteria. PLoS Genet. 7, e1002123.

Delarue, M., Brittingham, G.P., Pfeffer, S., Surovtsev, I.V., Pinglay, S., Kennedy, K.J.,

Schaffer, M., Gutierrez, J.I., Sang, D., Poterewicz, G., et al. (2018). mtorc1 controls phase separation and the biophysical properties of the cytoplasm by tuning crowding. Cell 174, 338–349.e20.

Espéli, O., Borne, R., Dupaigne, P., Thiel, A., Gigant, E., Mercier, R., and Boccard, F. (2012). A MatP-divisome interaction coordinates chromosome segregation with cell division in E. coli. EMBO J. 31, 3198–3211.

Espeli, O., Mercier, R., and Boccard, F. (2008). DNA dynamics vary according to macrodomain topography in the E. coli chromosome. Mol. Microbiol. 68, 1418–1427.

Folsom, J.P., Parker, A.E., and Carlson, R.P. (2014). Physiological and proteomic analysis of escherichia coli iron-limited chemostat growth. J. Bacteriol. 196, 2748–2761.

Greco, W.R., Bravo, G., and Parsons, J.C. (1995). The search for synergy: a critical review from a response surface perespective. Phar. Rev. 47, 331–385.

Greulich, P., Scott, M., Evans, M.R., and Allen, R.J. (2015). Growth-dependent bacterial susceptibility to ribosome-targeting antibiotics. Mol. Syst. Biol. 11, 796.

Gupta, R.S. (2011). Origin of diderm (Gram-negative) bacteria: antibiotic selection pressure rather than endosymbiosis likely led to the evolution of bacterial cells with two membranes. Antonie van Leeuwenhoek 100, 171–182.

Hardy, C.D., and Cozzarelli, N.R. (2003). Alteration of Escherichia coli topoisomerase IV to novobiocin resistance. Antimicrob. Agents Chemother. 47, 941–947.

Hoffman, L.R., D'Argenio, D.A., MacCoss, M.J., Zhang, Z., Jones, R.A., and Miller, S.I. (2005). Aminoglycoside antibiotics induce bacterial biofilm formation. Nature 436, 1171–1175.

Javer, A., Kuwada, N.J., Long, Z., Benza, V.G., Dorfman, K.D., Wiggins, P.a., Cicuta, P., and Lagomarsino, M.C. (2014). Persistent super-diffusive motion of Escherichia coli chromosomal loci. Nat. Commun. *5*, 3854.

Javer, A., Long, Z., Nugent, E., Grisi, M., Siriwatwetchakul, K., Dorfman, K.D., Cicuta, P., and Cosentino Lagomarsino, M. (2013). Short-time movement of E. coli chromosomal loci depends on coordinate and subcellular localization. Nat. Commun. *4*, 3003.

Jerman, B., Butala, M., and Zgur-Bertok, D. (2005). Sublethal concentrations of ciprofloxacin induce bacteriocin synthesis in Escherichia coli. Antimicrob. Agents Chemother. *49*, 3087–3090.

Joyner, R.P., Tang, J.H., Helenius, J., Dultz, E., Brune, C., Holt, L.J., Huet, S., Müller, D.J., and Weis, K. (2016). A glucose-starvation response regulates the diffusion of macromolecules. Elife *5*, 1–26.

Khil, P.P., and Camerini-Otero, R.D. (2002). Over 1000 genes are involved in the DNA damage response of Escherichia coli. Mol. Microbiol. *44*, 89–105.

Klumpp, S., and Hwa, T. (2008). Growth-rate-dependent partitioning of RNA polymerases in bacteria. Proc. Natl. Acad. Sci. U S A *105*, 20245–20250.

Klumpp, S., and Hwa, T. (2014). Bacterial growth: global effects on gene expression, growth feedback and proteome partition. Curr. Opin. Biotechnol. *28*, 96–102.

Konopka, M.C., Shkel, I.A., Cayley, S., Record, M.T., and Weisshaar, J.C. (2006). Crowding and confinement effects on protein diffusion in vivo. J. Bacteriol. *188*, 6115–6123.

Konopka, M.C., Sochacki, K.A., Bratton, B.P., Shkel, I.A., Record, M.T., and Weisshaar, J.C. (2009). Cytoplasmic protein mobility in osmotically stressed Escherichia coli. J. Bacteriol. *91*, 231–237.

Kwon, Y.K., Higgins, M.B., and Rabinowitz, J.D. (2010). Antifolate-induced depletion of intracellular glycine and purines inhibits thymineless death in E. coli. ACS Chem. Biol. *5*, 787–795.

Lampo, T.J., Kennard, A.S., and Spakowitz, A.J. (2016). Physical modeling of dynamic coupling between chromosomal loci. Biophys. J. *110*, 338–347.

Lin, J.T., Connelly, M.B., Amolo, C., Yaver, D.S., and Otani, S. (2005). Global transcriptional response of bacillus subtilis to treatment with subinhibitory concentrations of antibiotics that inhibit protein synthesis. Antimicrob. Agents Chemother. *49*, 1915–1926.

Long, C.P., Gonzalez, J.E., Sandoval, N.R., and Antoniewicz, M.R. (2016). Characterization of physiological responses to 22 gene knockouts in escherichia coli central carbon metabolism. Metab. Eng. *37*, 102–113.

Marquis, R.E. (1973). Immersion refractometry of isolated bacterial cell walls. J. Bacteriol. *116*, 1273–1279.

Michael, B., Lieberman, T.D., Kelsic, E.D., Chait, R., Gross, R., Yelin, I., and Kishony, R. (2016).

Spatiotemporal microbial evolution on antibiotic landscapes. Science *353*, 1147–1152.

Miermont, A., Waharte, F., Hu, S., McClean, M., Bottani, S., Léon, S., and Hersen, P. (2013). Severe osmotic compression triggers a slowdown of intracellular signaling, which can be explained by molecular crowding. Proc. Natl. Acad. Sci. U S A *110*, 5725–5730.

Mitosch, K., and Bollenbach, T. (2014). Bacterial responses to antibiotics and their combinations. Environ. Microbiol. Rep. *6*, 545–557.

Oldewurtel, E.R., Kitahara, Y., Cordier, B., Özbaykal, G., and van Teeffelen, S. (2019). Bacteria control cell volume by coupling cell-surface expansion to dry-mass growth. bioRxiv. . https://www.biorxiv.org/content/early/2019/09/16/769786. https://www.biorxiv.org/content/early/2019/09/16/769786.full.pdf.arXiv. https://doi.org/10.1101/769786.

Parry, B.R., Surovtsev, I.V., Cabeen, M.T., O'Hern, C.S., Dufresne, E.R., and Jacobs-Wagner, C. (2014). The bacterial cytoplasm has glass-like properties and is fluidized by metabolic activity. Cell *156*, 183–194.

Pelletier, J., Halvorsen, K., Ha, B.Y., Paparcone, R., Sandler, S., Woldringh, C., Wong, W., and Jun, S. (2012). Physical manipulation of the escherichia coli chromosome reveals its soft nature. Proc. Natl. Acad. Sci. U S A *109*, E2649–E2656.

Polovnikov, K.E., Gherardi, M., Cosentino-Lagomarsino, M., and Tamm, M.V. (2018). Fractal folding and medium viscoelasticity contribute jointly to chromosome dynamics. Phys. Rev. Lett. *120*, 088101.

Rahal, J.J., and Simberkoff, M.S. (1979). Bactericidal and bacteriostatic action of chloramphenicol against meningeal pathogens. Antimicrob. Agents Chemother. *16*, 13–18.

Ren, Q., Henes, B., Fairhead, M., and Thöny-Meyer, L. (2013). High level production of tyrosinase in recombinant escherichia coli. BMC Biotechnol. *13*, 18.

Rojas, E., Theriot, J.A., and Huang, K.C. (2014). Response of Escherichia coli growth rate to osmotic shock. Proc. Natl. Acad. Sci. U S A *111*, 7807–7812.

Rojas, E.R., Billings, G., Odermatt, P.D., Auer, G.K., Zhu, L., Miguel, A., Chang, F., Weibel, D.B., Theriot, J.A., and Huang, K.C. (2018). The outer membrane is an essential load-bearing element in gram-negative bacteria. Nature *559*, 617–621.

Scott, M., Gunderson, C.W., Mateescu, E.M., Zhang, Z., and Hwa, T. (2010). Interdependence of cell growth and gene expression: origins and consequences. Science *330*, 1099–1102.

Scott, M., Klumpp, S., Mateescu, E.M., and Hwa, T. (2014). Emergence of robust growth laws from optimal regulation of ribosome synthesis. Mol. Syst. Biol. *10*, 747.

Shaw, K.J., Miller, N., Liu, X., Lerner, D., Wam, J., Bittner, A., and Morrow, B. (2003). Comparison of the changes in global gene expression of Escherichia coli induced by four bactericidal agents. J. Mol. Microbiol. Biotechnol. *5*, 105–122.

Sobetzko, P., Travers, A., and Muskhelishvili, G. (2012). Gene order and chromosome dynamics coordinate spatiotemporal gene expression during the bacterial growth cycle. Proc. Natl. Acad. Sci. U S A *109*, 42–50.

Stavans, J., and Oppenheim, A. (2006). DNA-protein interactions and bacterial chromosome architecture. Phys. Biol. *3*, 1–10.

Stevenson, K., McVey, A.F., Clark, I.B.N., Swain, P.S., and Pilizota, T. (2016). General calibration of microbial growth in microplate readers. Sci. Rep. *6*, 38828.

Tsai, H., Nelliat, A., Choudhury, M., Kucharavy, A., Bradford, W.D., Cook, M.E., Kim, J., Mair, D.B., Sun, S.X., Schatz, M.C., and Li, R. (2019). Hypo-osmotic-like stress underlies general cellular defects of aneuploidy. Nature *570*, 117–121.

Tuomanen, E., Cozens, R., Tosch, W., Zak, O., and Tomasz, A. (1986). The rate of killing of Escherichia coli by beta-lactam antibiotics is strictly proportional to the rate of bacterial growth. J. Gen. Microbiol. *132*, 1297–1304.

Valkenburg, J., and Woldringh, C. (1984). Phase separation between nucleoid and cytoplasm in *Escherichia coli* as defined by immersive refractometry. J. Bacteriol. *160*, 1151–1157.

Waigh, T.A. (2005). Microrheology of complex fluids. Rep. Prog. Phys. *68*, 685–742.

Weber, S.C., Spakowitz, A.J., and Theriot, J.A. (2010a). Bacterial chromosomal loci move subdiffusively through a viscoelastic cytoplasm. Phys. Rev. Lett. *104*, 27–30.

Weber, S.C., Theriot, J.A., and Spakowitz, A.J. (2010b). Subdiffusive motion of a polymer composed of subdiffusive monomers. Phys. Rev. E Stat. Nonlin Soft Matter Phys. *82*, 011913.

Weber, S.C., Spakowitz, A.J., and Theriot, J.A. (2012). Nonthermal ATP-dependent fluctuations contribute to the in vivo motion of chromosomal loci. Proc. Natl. Acad. Sci. U S A *109*, 7338–7343.

Wiegand, I., Hilpert, K., and Hancock, R.E.W. (2008). Agar and broth dilution methods to determine the minimal inhibitory concentration (MIC) of antimicrobial substances. Nat. Protoc. *3*, 163–175.

Wlodarski, M., Raciti, B., Kotar, J., Cosentino Lagomarsino, M., Fraser, G.M., and Cicuta, P. (2017). Both genome and cytosol dynamics change in E. coli challenged with sublethal rifampicin. Phys. Biol. *14*, 015005.

Wood, J.M. (2006). Osmosensing by bacteria. Sci. Signal. *2006*, pe43.

Wood, T.K., Knabel, S.J., and Kwan, B.W. (2013). Bacterial persister cell formation and dormancy. Appl. Environ. Microbiol. *79*, 7116–7121.

You, C., Okano, H., Hui, S., Zhang, Z., Kim, M., Gunderson, C.W., Wang, Y.P., Lenz, P., Yan, D., and Hwa, T. (2013). Coordination of bacterial proteome with metabolism by cyclic amp signalling. Nature *500*, 301–306.

Yu, S., Sheats, J., Cicuta, P., Sclavi, B., Cosentino Lagomarsino, M., and Dorfman, K.D. (2018). Subdiffusion of loci and cytoplasmic particles are different in compressed cells. Commun. Biol. *1*, 176.

Supplemental Information

Cytosolic Crowding Drives the Dynamics

of Both Genome and Cytosol in *Escherichia coli*

Challenged with Sub-lethal Antibiotic Treatments

Michal Wlodarski, Leonardo Mancini, Bianca Raciti, Bianca Sclavi, Marco Cosentino Lagomarsino, and Pietro Cicuta

Supplementary materials of: Cytosolic crowding drives the dynamics of both genome and cytosol in *Escherichia coli* challenged with sublethal antibiotic treatments

Michal Wlodarski*

Biological and Soft Systems, Cavendish Laboratory, University of Cambridge, United Kingdom

Leonardo Mancini*

Biological and Soft Systems, Cavendish Laboratory, University of Cambridge, United Kingdom

Bianca Raciti

Biological and Soft Systems, Cavendish Laboratory, University of Cambridge, United Kingdom

Bianca Sclavi

Laboratory of Biology and Applied Pharmacology (UMR 8113 CNRS), École Normale Supérieure, Paris-Saclay, France

Marco Cosentino Lagomarsino**

Laboratory of Computational and Quantitative Biology (UMR 7238 CNRS), Sorbonne Université, Paris, France;

Pietro Cicuta**

Biological and Soft Systems, Cavendish Laboratory, University of Cambridge, United Kingdom

[a]IFOM Foundation FIRC Institute of Molecular Oncology Foundation, Milan 20139, Italy;
[b]Dipartimento di Fisica and I.N.F.N., Università degli Studi di Milano, Via Celoria 16, I-20133 Milano, Italy.

---

*Equal contribution
**Corresponding author
Email addresses: marco.cosentino-lagomarsino@ifom.eu
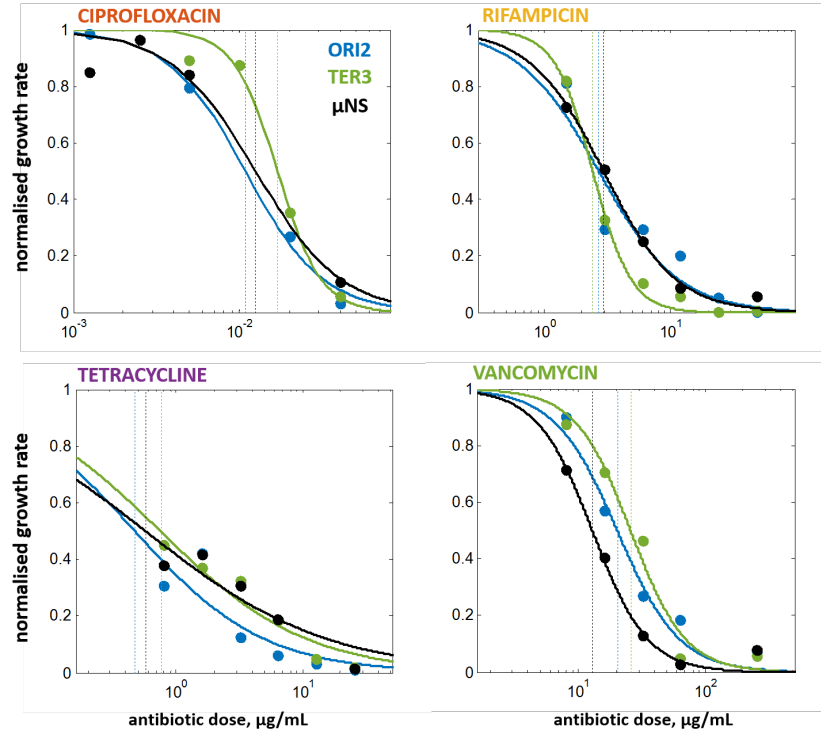(Marco Cosentino Lagomarsino), pc245@cam.ac.uk (Pietro Cicuta)

Figure S1: **Dose-response curves used for the IC_{50} concentrations determination, related to Figure 1.** Slopes of the linear parts of the growth curves obtained at varying concentrations of antibiotics were calculated and the means were used to construct the dose-response curves. After fitting with Equation S1, IC_{50} concentrations (*dashed vertical lines*) were selected experiments (Table S3). Curve colours represent tested strains: Ori2 (*blue*), Ter3 (*green*), and μNS (*black*).
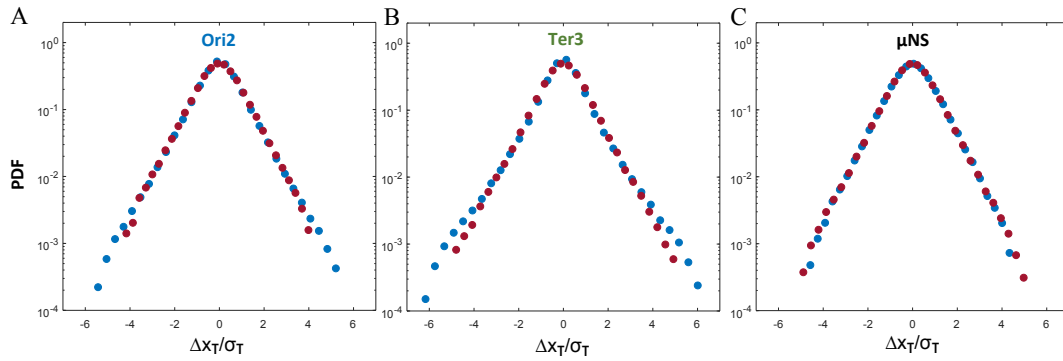

Figure S2: **Step-size distributions for $\tau = 0.1$ s after 1 h treatment with sorbitol, related to Figure 2.** Panels show normalised probability distributions of step sizes at τ=0.1 s along a fixed x-direction normalised by standard deviation for **(A)** Ori2 and **(B)** Ter3 chromosomal loci, and **(C)** cytosolic μNS aggregates, tracked on agar. Data is binned into an arbitrary number of 32 linearly spaced out bins; bins containing at least 50 steps are shown. No significant difference between the control and sorbitol-treated data was observed.
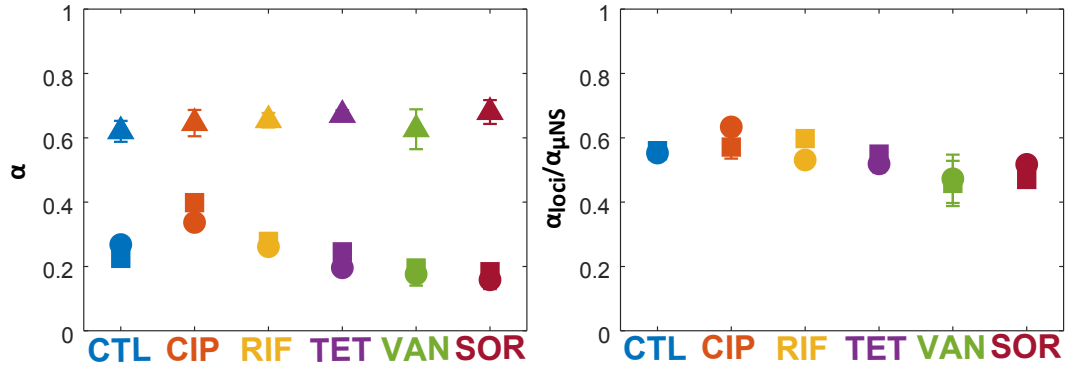
Figure S3: **Some of the treatment conditions change the scaling exponent** α**, related to Figure 2.** The *left* panel shows the scaling exponent α for all tested treatments at $T_{treat} = 20$ min (Ori2, *circles*; Ter3, *squares*; μNS, *triangles*). Error bars show the standard deviations of the medians of the distributions divided by the square root of the number of biological replicates ($n = 9$ and 6 for chromosomal and cytosolic markers, respectively); in most cases the error bars are smaller than the plot markers. The *right* panel shows the loci/μNS ratios of the scaling exponents (Ori2/μNS, *circles*; Ter3/μNS, *squares*. The error bars represent propagated standard deviations. The antibiotic-induced changes to α observed in this work are much smaller (change of up to 16% at the shortest T_{treat}) compared those in compressed cells (change of at least 20% at 20 psi for all markers, as reported previously by Shi et al. (Yu et al., 2018)).
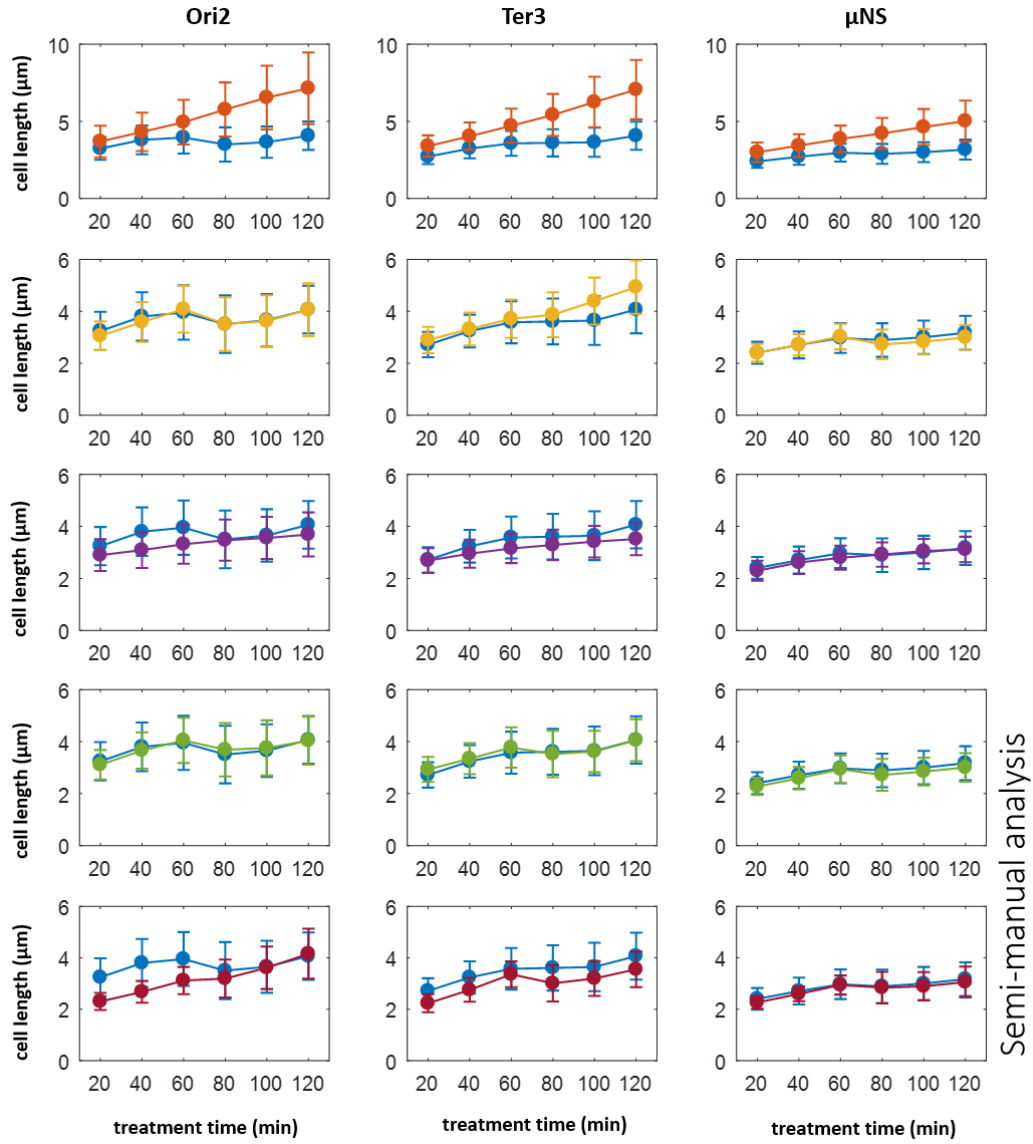
Figure S4: **Cell lengths measured semi-manually, related to Figure 5.** Strains are indicated at the top of each column of plots; treated with ciprofloxacin (*orange*), rifampicin (*yellow*), tetracycline (*violet*), vancomycin (*green*), and sorbitol (*red*); and the controls (*blue*).
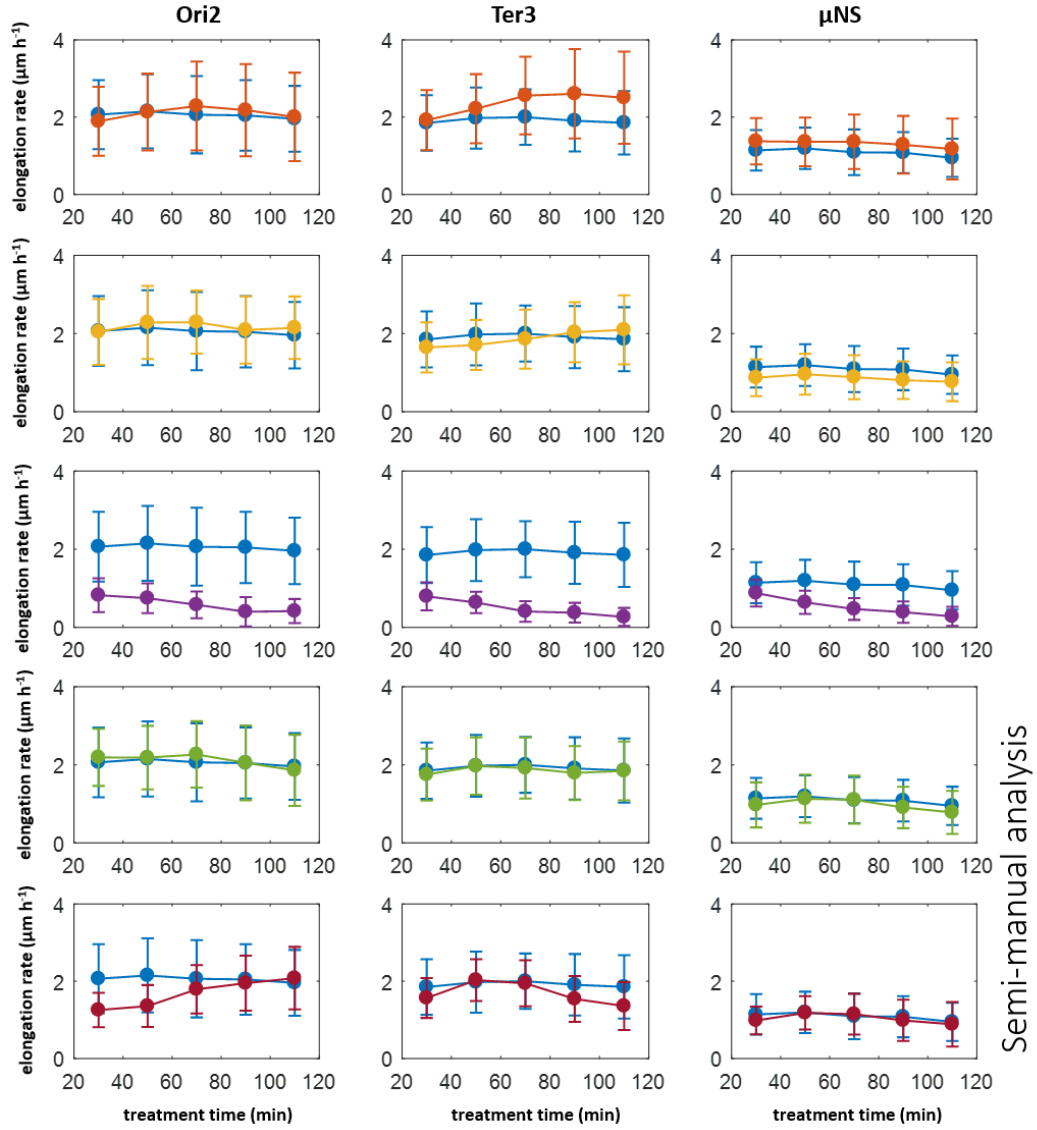
Figure S5: **Cell elongation rates measured semi-manually, related to Figure 5.** Strains are indicated at the top of each column of plots; treated with ciprofloxacin (*orange*), rifampicin (*yellow*), tetracycline (*violet*), vancomycin (*green*), and sorbitol (*red*); and the controls (*blue*).

Figure S6: **Cell lengths measured with SuperSegger software, related to Figure 5.** Strains are indicated at the top of each column of plots; treated with ciprofloxacin (*orange*), rifampicin (*yellow*), tetracycline (*violet*), vancomycin (*green*), and sorbitol (*red*); and the controls (*blue*).
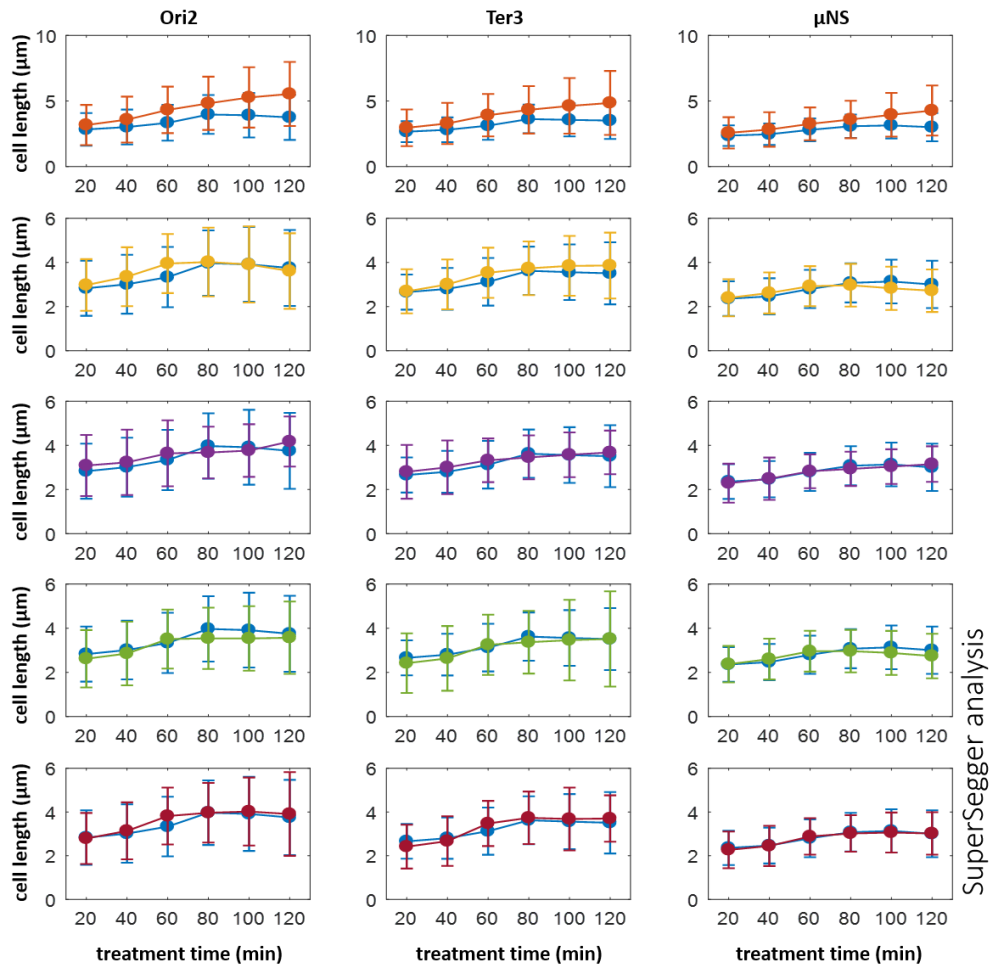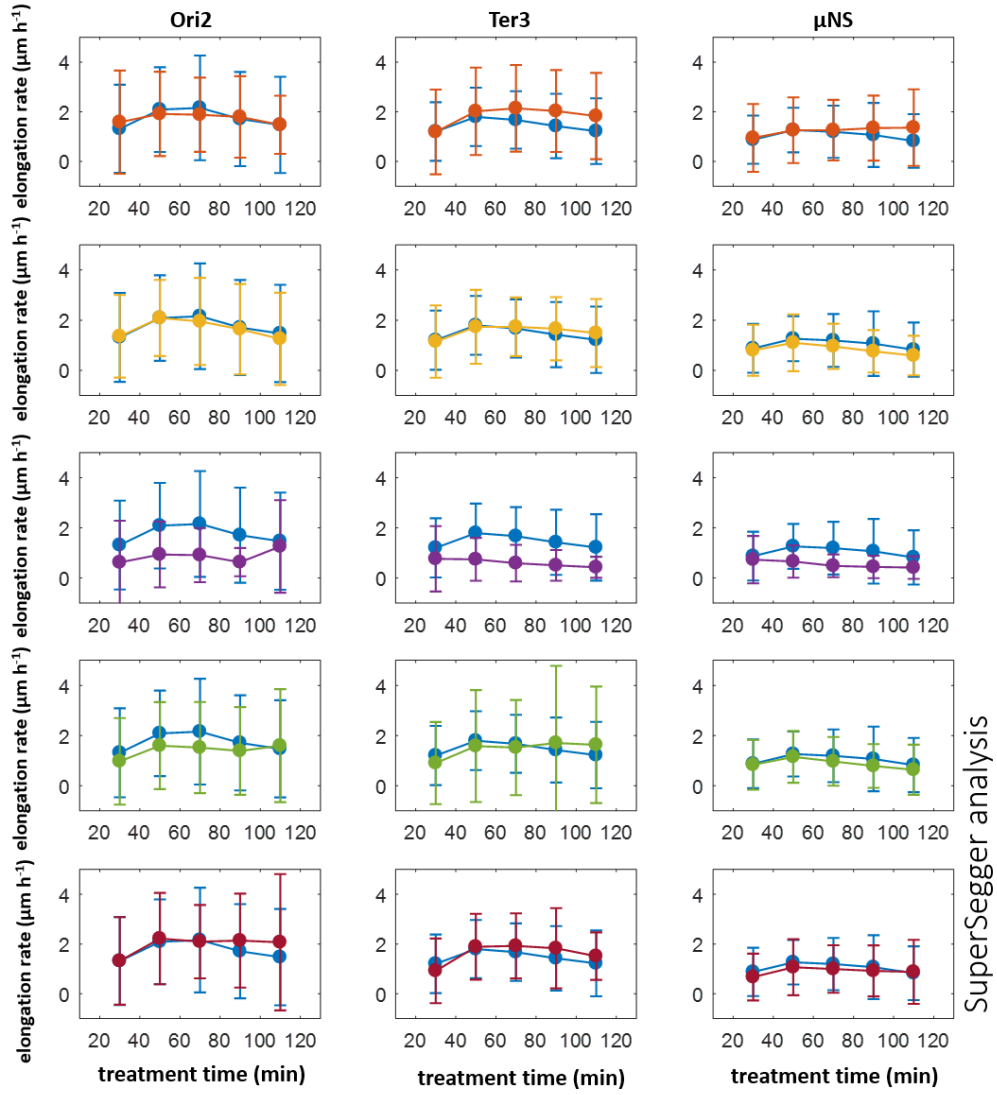
Figure S7: **Cell elongation rates measured with SuperSegger software, related to Figure 5.** Strains are indicated at the top of each column of plots; treated with ciprofloxacin (*orange*), rifampicin (*yellow*), tetracycline (*violet*), vancomycin (*green*), and sorbitol (*red*); and the controls (*blue*).
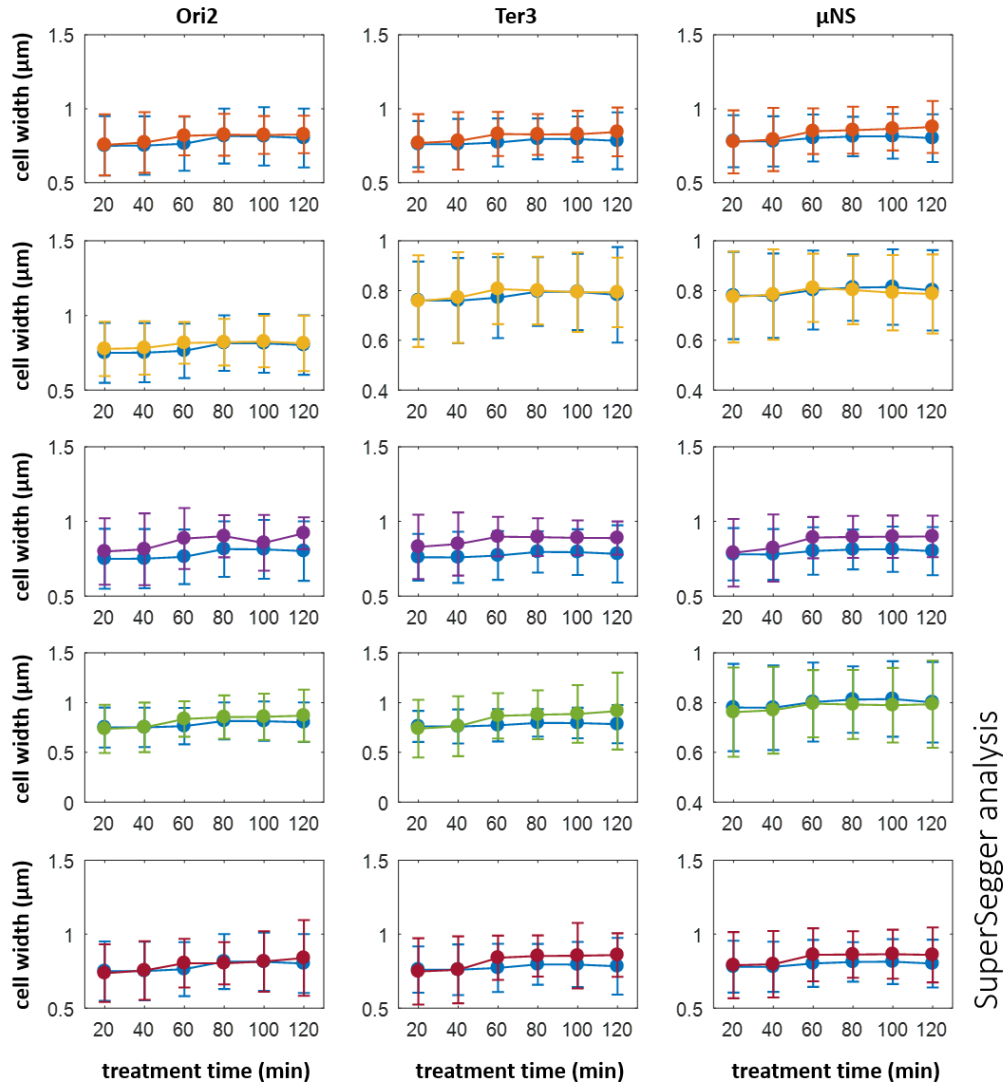
Figure S8: **Cell widths measured with SuperSegger software, related to Figure 5.** Strains are indicated at the top of each column of plots; treated with ciprofloxacin (*orange*), rifampicin (*yellow*), tetracycline (*violet*), vancomycin (*green*), and sorbitol (*red*); and the controls (*blue*).

marker	experiment #	bio. repl.	control	ciprofloxacin	rifampicin	tetracycline	vancomycin	sorbitol
Ori2	1.	3	7,985	5,015	1,986	451	2,608	1,356
	2.	3	4,051	2,556	3,443	712	2,110	338
	3.	3	1,728	1,977	2,528	2,768	1,356	2,001
	subtotals	*3*	*9*	*13,764*	*9,548*	*7,957*	*3,931*	*6,074*	*3,695*
Ter3	4.	3	1,456	3,387	4,718	1,440	1,342	868
	5.	3	3,214	3,199	3,499	2,560	2,698	454
	6.	3	1,694	1,813	2,649	1,243	3,601	888
	subtotals	*3*	*9*	*6,364*	*8,399*	*10,866*	*5,243*	*7,641*	*2,210*
GFP-µNS	7.	3	1,230	841	784	10,66	746	1,837
	8.	3	760	743	1,127	298	1,078	948
	subtotals	*2*	*6*	*1,990*	*1,584*	*1,911*	*1,364*	*1,824*	*2,785*
97,150	*TOTALS*	*8*	*24*	*22,118*	*19,531*	*20,734*	*10,538*	*15,539*	*8,690*

Table S1: **Number of collected and analysed tracks and biological replicates for individual experiments, related to Figure 1.** Numbers represent sums of tracks acquired at all measurement time points (6 every 20 min). For each marker type, three experiments – each for 3 (chromosomal loci) or 2 (cytosolic aggregates) biological replicates (refer to Section 1.2 of Methods for details) were completed. In total, at least 1,364 (µNS, tetracycline) and up to 13,764 (Ori2, control) tracks were collected per treatment condition. The total of 97,150 tracks were collected and analysed for entire work.
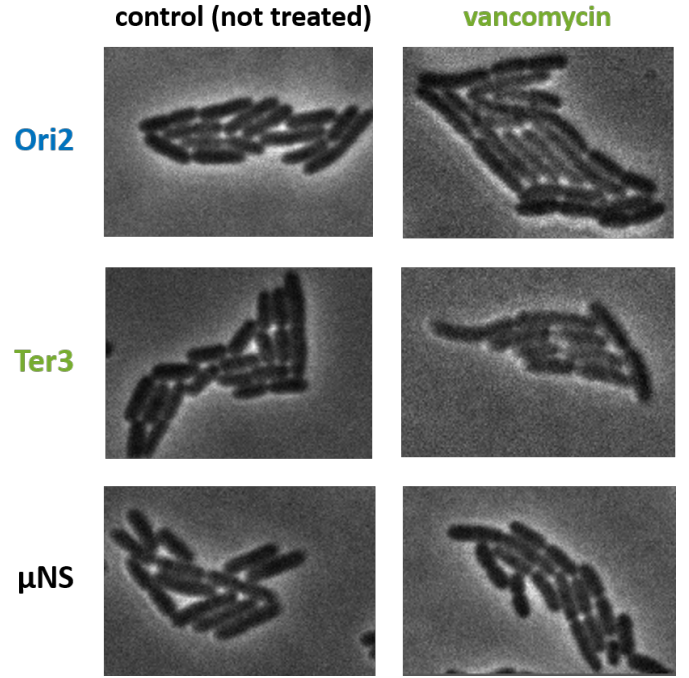

Figure S9: **Vancomycin changes cell morphology, related to Figure 5.** Example phase contrast images of three *E. coli* strains under no treatment and sub-lethal vancomycin. Treatment with vancomycin affects cell shape causing unusual bending of cells.
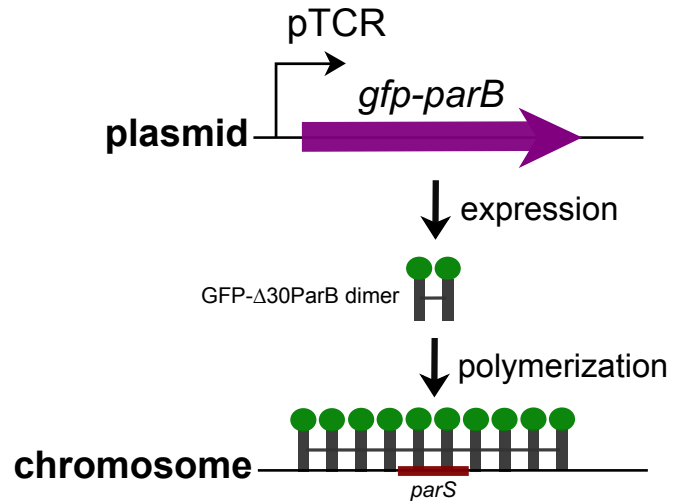

Figure S10: **Schematic representation of the ParB-*parS* chromosomal loci labelling system, related to Figure 1.** Expression of the plasmid-based fluorescent *gfp-parB* fusion protein is under control of an ITPG-inducible pTCR promoter. The truncated Δ30 ParB protein fused to GFP forms a dimer in solution but polymerases when bound to the chromosomal *parS* binding site, forming a trackable fluorescent marker.

Treatment	Ori2 p-value	Ter3 p-value	Cyt p-value
Ciprofloxacin	0.003	<0.001	<0.001
Rifampicin	0.614	0.028	0.168
Tetracycline	0.619	0.025	0.292
Vancomycin	<0.001	0.016	0.048
Sorbitol	<0.001	<0.001	<0.001

Table S2: **Statistical significance of the changes in MSD shown in Fig. 1 of the main text, related to Figure 1.** The MSD of the markers shown remains overall constant over treatment time as shown in Figure 1 such that trends can be fitted by straight lines parallel to the x axis, with a constant y value equal to the mean of the data points over time. Because every data point is in turn the result of the average of the medians of different biological replicates, each median was considered representative of MSD and the statistical significance of their changes assayed with a t-test. P-values are given.
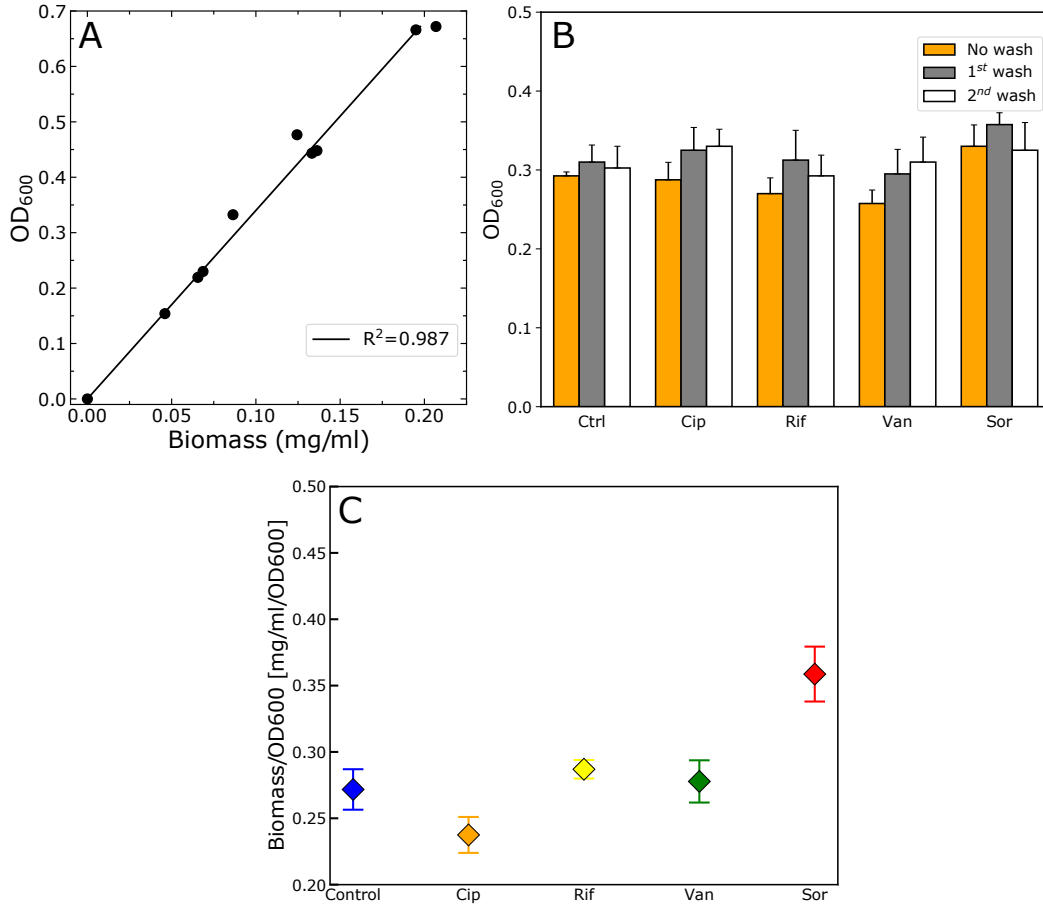

Figure S11: **Measurements of optical density and dry mass enable the estimation of cell density variations, related to Figure 5.** (**A**) OD_{600} to dry mass linear correlation for untreated cells. Results from 3 biological replicates. To ensure that the correlation was assayed for cells with the same properties, each sample was collected and used to produce 3 dilutions: 1:0, 2:3 and 1:3. (**B**) Washing of the samples via centrifugation and resuspension in water does not cause differential cell lysis. Optical density of unwashed cells (orange), cells washed once in water (grey) and cells washed twice in water (white) are given. Bars are the average of 4 replicates and the error bars show the standard deviation. (**C**) Experiments presented in Figure 6A of the main text were repeated on ice to exclude artifacts due to cell growth during sample handling. Data points show the average of 3 replicates with the error bars showing the standard deviation.
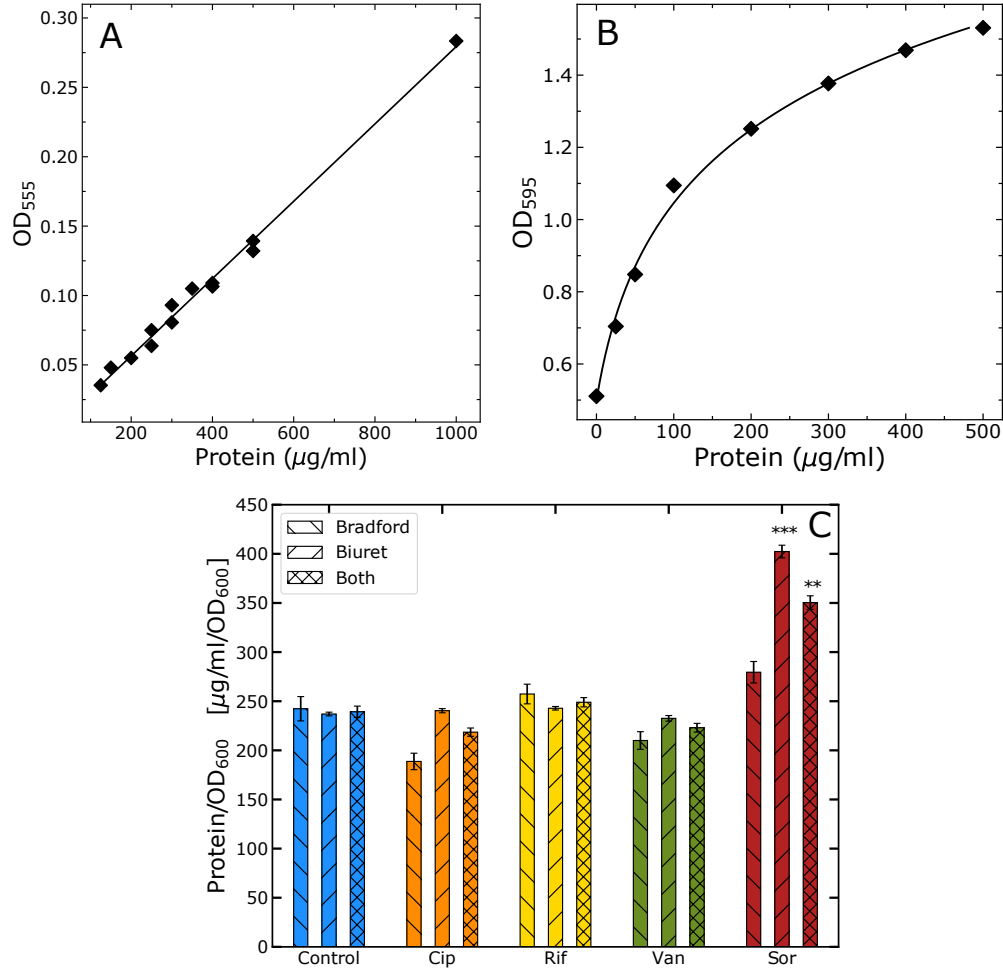
Figure S12: **Comparison of protein estimation results from the Biuret and Bradford assays, related to Figure 5.** (**A**) Biuret assay calibration curve with BSA protein. Data was fitted to a straight line: $aProtein + b$ where a = 0.00028 and b = 0.0007 are fitting parameters. (**B**) Bradford assay calibration curve with BSA protein. Data was fitted to a logarithmic curve: $alog_2(b + Protein) + c$, where a = 0.241, b = 26.231, c = -0.64 are fitting parameters. (**C**) Comparison of protein concentration estimation for the two assays (Bradford and Biuret) and for the results of both combined (Both). Statistical significance of the differences was estimated with a t-test and p-value significance is given.

1. TRANSPARENT METHODS

1.1. Strains

To investigate chromosomal dynamics, building on previous studies (Javer et al., 2013, 2014; Wlodarski et al., 2017), we used two *E. coli* MG1655 strains with the GFP-ParB/*parS* fluorescent labelling system (kindly provided by Dr Olivier Espéli and Dr Frédéric Boccard (Rocha, 2008)). In each of these strains a P1 *parS* site inserted at either Ori2 or Ter3 positions on the chromosome (3,928,826 and 1,341,067 chromosomal coordinates, respectively). Loci have names assigned according to the MD they belong to. Expression of the ParB-GFP fusion protein is driven by a leaky promoter on the pALA2705 plasmid (Figure S10). No isopropyl β-D-1-thiogalactopyranoside (IPTG) induction was required to produce the ParB-GFP levels necessary to visualize and track loci.

To investigate cytosolic dynamics we used the *E. coli* CJW4617 strain (kindly provided by Christine Jacobs-Wagner's laboratory) of a MG1655 background capable of expressing μNS-GFP fusion protein. The avian reovirus protein μNS is a self-assembling protein (Broering et al., 2002) and its C-terminal fragment can form globular cytoplasmic particles, even when fused to GFP (Broering et al., 2005). μNS-GFP synthesis is under control of the chromosomal IPTG-inducible promoter lac. In this strain, the lactose/IPTG permease-encoding, lacY gene is deleted from the lac operon. Crucially, μNS-GFP aggregates are unlikely to make specific interactions with components of the bacterial cytoplasm, given the evolutionary divergence between bacteria and the avian reovirus. We induced the synthesis of the aggregates with 1 mM IPTG for 3.5-4 h, centrifuged the culture at 4,000 rpm for 10 min, and stopped induction by washing the pellet with the growth medium directly before experiments. Induction of GFP-μNS synthesis usually resulted in a single fluorescent focus per cell.

1.2. Culture conditions

All chemical reagents were obtained from Sigma-Aldrich unless otherwise stated. For all microscopy experiments, we used the "minimal medium" consisting of M9 minimal salts (BD) supplemented with complementary salts (CS; MgSO$_4$ 2 mM, CaCl$_2$ 100 μM, tryptophan 4 μg/mL, and thymidine 5 μg/mL), 0.4% glucose (Glu), and 0.5% casamino acids (CAAs; BD). Strains were stored at -80°C in lysogeny broth (LB) +25% glycerol stocks and were streaked on LB plates (containing relevant antibiotic for selection: ampicillin 100 μg/mL and chloramphenicol 25 μg/mL). From each plate, bacteria from 3-4 distinct colonies were selected to inoculate the growth medium and strains were grown overnight at 37°C in LB with ampicillin 100 μg/mL, with shaking at 200 rpm at a 45° angle. Overnight cultures were diluted 1:200 into 2 mL of fresh minimal medium (with no antibiotic) and grown at 30°C to the optical density at a 600 nm wavelength (OD$_{600}$) of 0.2-0.3 (early exponential growth phase) and transferred onto agarose pads

	Agarose pads		Liquid (bulk) culture (IC$_{50}$)
	Determined MIC range	Tested concentration (~75% of MIC)	
ciprofloxacin	0.012-0.014 µg/mL	0.01 µg/mL (0.3 µM)	Ori2: 0.011 µg/mL (0.033 µM) Ter3: 0.016 µg/mL (0.048 µM) µNS: 0.013 µg/mL (0.039 µM)
rifampicin	1.2-1.4 µg/mL	1.0 µg/mL (1.2 µM)	Ori2: 2.7 µg/mL (3.3 µM) Ter3: 2.4 µg/mL (2.9 µM) µNS: 2.9 µg/mL (3.5 µM)
tetracycline	0.8-1.0 µg/mL	0.7 µg/mL (1.6 µM)	Ori2: 0.47 µg/mL (1.1 µM) Ter3: 0.75 µg/mL (1.7 µM) µNS: 0.57 µg/mL (1.3 µM)
vancomycin	32-36 µg/mL	25 µg/mL (17.3 µM)	Ori2: 20.3 µg/mL (14.0 µM) Ter3: 25.7 µg/mL (17.7 µM) µNS: 12.8 µg/mL (8.8 µM)
sorbitol	N/A	72.8 mg/mL (400 mM)	72.8 mg/mL (400 mM)

Table S3: **Antibiotic and sorbitol concentrations used in this work, related to Figure 1.** For agarose pad experiments, the MIC range for each antibiotic was determined for each of the three strains (MIC ranges did not differ between different strains). Tested sub-lethal concentrations were ~75% of the MIC. For the Bradford test, involving measurements on bulk cultures, dose-response curves were constructed (Figure S1) and fitted IC$_{50}$ concentrations were selected for experiments.

for image acquisition. Doubling times in bulk (at 37°C in the minimal medium with CAAs) were 65 min, Ori2 and Ter3 MG1655; 80 min, CJW4617. For the estimation of cell density, overnight cultures of the CJW4617 strain were diluted 1:200 in 250 ml Luria-Bertani (LB) broth (0.5% yeast extract, 1% Bacto Tryptone, 0.5% NaCl) with no antibiotic and grown at 37°C with 200 rpm shaking. Upon reaching an OD$_{600}$ of 0.1 - 0.3, the various antibiotics and sorbitol were added to the cultures and incubated for further 60 minutes before harvesting for optical density, dry mass and refractive index estimations.

1.3. Sample preparation for microscopy experiments

Agarose pads contained 1.5% w/v agarose dissolved in the minimal medium and (if required) a fixed concentration of an antibiotic. Pads were approximately 8 mm in diameter and 0.5 mm in thickness. 2.5 μL of the culture were deposited on a pad under aseptic conditions. The pad was then sealed between a cover slip and a glass slide with a stack of 3 frame seals (Fisher Scientific) to ensure access to excess of oxygen. Under the microscope, the sample was maintained at 30°C during image acquisition for 2 hours, waiting for 20 min before acquiring the first image. Doubling times (without treatment) on agarose pads were 45 min (Ori2 MG1655), 50 min (Ter3 MG1655), and 63 min (CJW4617) (all $\pm$ 10 min) measured for individual cells (about 550 cells per strain).

For temperature control, we used a custom built proportional–integral–derivative (PID) temperature controller with two output channels, developed by Dr Jurij Kotar. One channel is used for heating a microscope objective with a heat-

ing collar, the other channel is used for heating a Fluorine doped Tin Oxide (FTO) glass plate. A sample sits on the glass plate. Temperature is measured with K-type thermocouples.

1.4. Determining sub-lethal antibiotic concentrations

In all experiments, we treated bacteria with antibiotic concentrations capable of affecting significantly the cellular physiology but allowing for normal growth. The minimal inhibitory concentration (MIC) range for each antibiotic was determined for each of the three strains (MG1655 Ori2, MG1655 Ter3, and CJW4617 μNS) using a standard agar dilution MIC determinaton method (Wiegand et al., 2008). Determined MIC ranges did not differ between different strains. Tested sub-lethal concentrations were ~75% of the MIC (Table S3). Sorbitol was tested at a 400 mM concentration, capable of inducing a hyperosmotic shock in *E. coli* as reported previously (Rojas et al., 2014). As agarose pads can absorb liquid, it is possible that dissolved antibiotic was diluted after loading the pad with culture. The volume of an agarose pad was about 25 μL and the volume of the loaded culture was 2.5 μL resulting in an up to a ×1.1 dilution. However, a smaller dilution is likely as some of the loaded culture evaporated rather then being absorbed into the pad.

Dose response curves were obtained for the Bradford test using a FLUOstar OMEGA 96-well plate reader (BMG Labtech). Bacteria were grown at 30°C after diluting overnight cultures 200:1 into 300 μL of minimal medium containing a range of antibiotic concentrations, and measuring the OD$_{600}$ every 30 min for 12 h with shaking at 200 rpm. The slopes of the linear parts of the growth curves from at least 4 biological replicates were calculated and the means used to construct the dose-response curves (Figure S1), fitted with Equation S1:

$$g(c) = \frac{g_0}{1 + \frac{c}{IC_{50}}}, \tag{S1}$$

where g is growth rate, g_0 is the growth rate without antibiotic, c is antibiotic concentration, and IC_{50} is the fitted IC_{50} concentration, selected for experiments (Table S3).

1.5. Image acquisition and processing

1.5.1. Equipment specifications.

We used a Nikon Eclipse TiE inverted microscope with a 60× oil immersion objective (NA=1.45). Images were further magnified with a 2.5× TV adapter before detection on an Andor iXon EM-CCD camera, capable of detecting single fluorophores and yielding a high signal-to-noise ratio to enable high marker localisation precision. Blue LED with a 470 nm peak and 20 nm spectral width was used to excite the GFP using a Semrock LED-FI filter with the exciter 474 nm (25 nm spectral width), dichroic 495 nm, and emitter 515 nm (25 nm spectral width) bands. Focus during image acquisition was maintained with the Nikon perfect focus system (PFS).

1.5.2. Image acquisition.

For marker tracking, 21 manually selected fields of view were scanned, each field of view containing about 30 fluorescent markers. 45 s movies were acquired at a 9.6 frame-per-second frame rate with an exposure time of 104 ms. In addition to the movie acquired in the fluoresence mode, a phase contrast image, and a dark frame (acquired immediately before the fluorescent image acquisition using identical settings but no illumination) of each field of view were acquired at every scan. During experiments, each field of view was scanned 6 times, 20 min apart (total scanning time 2 h).

1.5.3. Image processing and data analysis.

First, the dark frame was subtracted from all other images. For marker dynamics analysis, image processing methods, tracking analysis, image feature extraction, and MSD fitting algorithms were identical to those previously developed and reported by Javer *et al.* (Javer et al., 2013). All image processing and data analysis including plotting the data were accomplished with custom-written programs using in-built and open-source functions of MATLAB® software, with occasional use of Python, ImageJ, IrfanView, and Inkscape.

1.6. Semi-manual cell size analysis

We performed semi-manual measurements of cell lengths and widths. The length of the long and short axis of individual bacteria were measured manually using built-in MATLAB® image display and coordinate marking functions (Figure S13). Cell length was calculated by determining the distance between two furthest points on the bacterium edge (marked on images in Figure S13C). For highest accuracy, all semi-manual measurements were performed by the same person and identical criteria were applied to determine cell boundaries for all measured cells across all treatment conditions.

Semi-manual cell size analysis of phase contrast images was further corroborated with the SuperSegger program designed for automated bacteria segmentation and lineage generation. For SuperSegger software features, capabilities and benchmarks refer to (Stylianidou et al., 2016), while for gating capabilities refer to (Cass et al., 2017).

1.7. Dry mass estimation

Cells grown to an OD$_{600}$ of 0.1-0.3 were treated with antibiotics or sorbitol for 60 minutes as explained above. Their dry mass was estimated as in (Basan et al., 2015). Briefly, sample OD$_{600}$ was recorded from diluted aliquots and the remaining culture centrifuged at 8000g for 10 minutes. The obtained pellet was washed in 200 ml of water, centrifuged again and the pellet re-suspended in 2 ml water. Samples were transferred onto pre-weighted aluminium boats, desiccated overnight at 70°C and weighted.
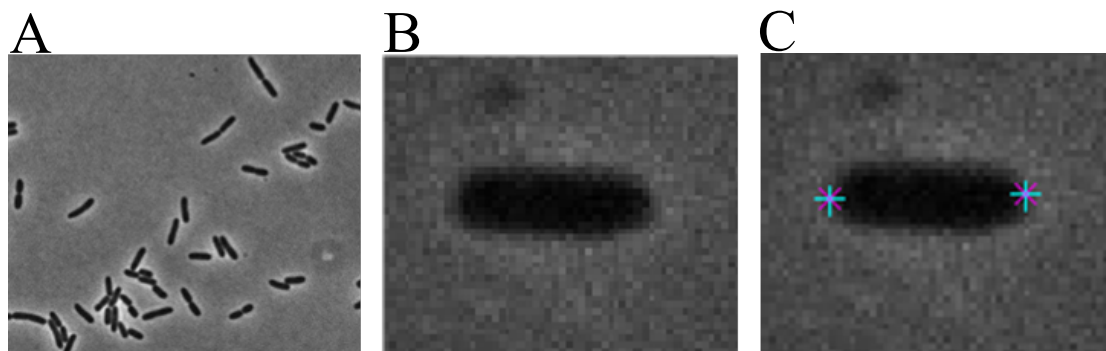
Figure S13: **Semi-manual single-cell level cell size measurements, related to Figure 5.** (**A**) Example images of *E. coli* in the phase contrast mode. (**B**) Images of individual cells were enlarged manually for higher measurement accuracy. (**C**) Length of each measured cell was determined by calculating the distance between two furthest points on the bacterium edge (marked on images with star symbols).

1.8. Refractive index estimation

The refractive index (RI) of treated and untreated cells was assayed by comparison with the one of bovine serum albumin (BSA) solutions as in (Marquis, 1973; Bateman et al., 1966). The OD of medium in which cells have been re-suspended matches the one of cell-free medium if medium and cells have the same RI. The addition of BSA changes the RI of solutions by a known amount which scales linearly with BSA concentration (Figure ??B, inset) (Barer and Tkaczyk, 1954; Crespi et al., 2012), such that the RI of cells can be simply inferred from the concentration of BSA necessary to make their optical density vanish. In our case, BSA (Sigma) was dissolved in water at a final concentration of 10, 20 and 30% in weight. NaCl was supplemented to these solutions in order to match the osmolarity of growth medium and limit artifacts due to osmotic effects that would alter cell size. Aliquots of treated and untreated cells were resuspended in the various BSA solutions, and their OD_{700} estimated.

1.9. Protein content estimation

To assay whether the changes in dry mass were due to changes in protein content, protein concentration was examined via two independent colorimetric assays: the Biuret and Bradford assays (see Figure S12, Supplementary Materials). The Biuret assay was carried out as in (You et al., 2013). Samples from treated and untreated cells were washed via centrifugation at 8000g for 2 minutes with 1 ml water, resupended in 0.5 ml water and freezed at -80°C. Samples were thawed at room temperature, 0.25 ml of a 3M NaOH solution were added and boiled at 100°C for 5 minutes. Samples were let to cool down at room temperature and 0.25 ml of 1.6% CuSO4 were added. Solutions were incubated at room temperature for 5 minutes and centrifuged at maximum speed. The optical density of the supernatant was assayed at $\lambda = 555$ nm and protein concentration calculated by comparison with calibration curves obtained by carrying out the assay on known concentrations of BSA. For the Bradford assay (Kruger, 2009),

pellet from samples washed in 1 ml water was re-suspended in 0.2 ml of B-PER^{TM} (Thermo Scientific) Bacterial Protein Extraction Reagent and shaken for 15 minutes at room temperature. Samples were then centrifuged at maximum speed for 2 minutes and the supernatant diluted 1:10 into Coomassie stain (Thermo Scientific). After further 10 minutes incubation at room temperature, the optical density of the samples was assayed at $\lambda = 595$ nm and compared to a calibration curve obtained from BSA dilutions.

References

Barer, R., Tkaczyk, S., 1954. Refractive index of concentrated protein solutions. Nature 173, 821–822.

Basan, M., Zhu, M., Dai, X., Warren, M., Sévin, D., Wang, Y.P., Hwa, T., 2015. Inflating bacterial cells by increased protein synthesis. Mol. Sys. Biol. 11, 836.

Bateman, J.B., Wagman, J., Carstensen, E.L., 1966. Refraction and absorption of light in bacterial suspensions. Kolloid-Zeitschrift und Zeitschrift für Polymere 208, 44–58.

Broering, T.J., Arnold, M.M., Miller, C.L., Hurt, J.A., Joyce, P.L., Nibert, M.L., 2005. Carboxyl-Proximal Regions of Reovirus Nonstructural Protein muNS Necessary and Sufficient for Forming Factory-Like Inclusions. J. Virol. 79, 6194–6206.

Broering, T.J., Parker, J.S.L., Joyce, P.L., Kim, J., Nibert, M.L., 2002. Mammalian Reovirus Nonstructural Protein NS Forms Large Inclusions and Colocalizes with Reovirus Microtubule-Associated Protein 2 in Transfected Cells. J. Virol. 76, 8285–8297.

Cass, J.A., Stylianidou, S., Kuwada, N.J., Traxler, B., Wiggins, P.A., 2017. Probing bacterial cell biology using image cytometry. Mol. Microbiol. 103, 818–828.

Crespi, A., Lobino, M., Matthews, J.C.F., Politi, A., Neal, C.R., Ramponi, R., Osellame, R., O'Brien, J.L., 2012. Measuring protein concentration with entangled photons. Appl. Phys. Lett. 100, 233704.

Javer, A., Kuwada, N.J., Long, Z., Benza, V.G., Dorfman, K.D., Wiggins, P.a., Cicuta, P., Lagomarsino, M.C., 2014. Persistent super-diffusive motion of Escherichia coli chromosomal loci. Nat. Commun. 5, 3854.

Javer, A., Long, Z., Nugent, E., Grisi, M., Siriwatwetchakul, K., Dorfman, K.D., Cicuta, P., Cosentino Lagomarsino, M., 2013. Short-time movement of E. coli chromosomal loci depends on coordinate and subcellular localization. Nat. Commun. 4, 3003.

Kruger, N.J., 2009. The Bradford Method For Protein Quantitation. Humana Press, Totowa, NJ. pp. 17–24.

Marquis, R.E., 1973. Immersion refractometry of isolated bacterial cell walls. J. Bacteriol. 116, 1273–1279.

Rocha, E.P.C., 2008. The organization of the bacterial genome. Annu. Rev. Genet. 42, 211–233.

Rojas, E., Theriot, J.A., Huang, K.C., 2014. Response of Escherichia coli growth rate to osmotic shock. Proc. Natl. Acad. Sci. U.S.A. 111, 7807–7812.

Stylianidou, S., Brennan, C., Nissen, S.B., Kuwada, N.J., Wiggins, P.A., 2016. SuperSegger: robust image segmentation, analysis and lineage tracking of bacterial cells. Mol. Microbiol. 102, 690–700.

Wiegand, I., Hilpert, K., Hancock, R.E.W., 2008. Agar and broth dilution methods to determine the minimal inhibitory concentration (MIC) of antimicrobial substances. Nat. Protoc. 3, 163–75.

Wlodarski, M., Raciti, B., Kotar, J., Cosentino Lagomarsino, M., Fraser, G.M., Cicuta, P., 2017. Both genome and cytosol dynamics change in E. coli challenged with sublethal rifampicin. Phys. Biol. 015005.

You, C., Okano, H., Hui, S., Zhang, Z., Kim, M., Gunderson, C.W., Wang, Y.P., Lenz, P., Yan, D., Hwa, T., 2013. Coordination of bacterial proteome with metabolism by cyclic amp signalling. Nature 500, 301–306.

Yu, S., Sheats, J., Cicuta, P., Sclavi, B., Cosentino Lagomarsino, M., Dorfman, K.D., 2018. Subdiffusion of loci and cytoplasmic particles are different in compressed cells. Communications biology 1, 176.